RESEARCH ARTICLE

DOI: 10.54926/jnamt.2025.247

J Nav Architect Mar Technol 2025;227(1):1-21

A Comprehensive CFD Analysis of Tandem Foils With and Without Ground Effect

Mehmet Delikan, Şakir Bal

İstanbul Technical University Faculty of Naval Architecture and Marine Sciences, Department of Naval Architecture and Ocean Engineering, İstanbul, Türkiye

To cite this article: M. Delikan, and Ş. Bal. A comprehensive CFD analysis of tandem foils with and without ground effect. *J Nav Architect Mar Technol*. 2025;227(1):1-21.

Received: 12.11.2024 - **Revised:** 10.02.2025 - **Accepted:** 05.03.2025 - **Publication Date:** 06.05.2025

Abstract

The flow dynamics and performance of tandem foils, both with and without ground effect (GE), continue to present challenges that are critical to understanding and optimizing aero/hydrodynamic systems, particularly for applications in next-generation wing-in-ground (WIG) effect vehicles, sailing yachts, and hydrofoil vessels. The performance of foils in GE (IGE) versus out of GE has not been extensively compared. This comprehensive study investigates the aero/hydrodynamic performance and flow dynamics of tandem foils using NACA 4412 section at moderate Reynolds number. To isolate the effects of spacing and ground clearance (H), both foils were set at a fixed angels of attack to negate the influence of decalage angle. The design variables examined include horizontal and vertical spacing between the foils, as well as H. Performance comparisons in both GE and out-of-GE conditions were presented, focusing on lift-to-drag ratio, lift and drag, and foil-to-foil interaction dynamics. Numerical simulations were conducted using the finite-volume method to solve the incompressible Reynolds-averaged-Navier-Stokes equations with the shear-stress transport k-ω turbulence model with gamma-transition model. Results indicate that the superiority of tandem foils is highly configuration-dependent. IGE, tandem foils exhibit a significantly higher lift-to-drag ratio than in out-of-GE conditions, where their performance is often lower than that of isolated foils. Positive G between the foils were found to enhance aero/hydrodynamic efficiency, suggesting that optimizing the gap distance can lead to performance improvements. The stagger distance plays a critical role in altering the static pressure distribution due to foil-to-foil interactions. Notably, under certain interference conditions, the fore foil can experience reduced drag or even generate thrust, offering potential advantages for specific aero/hydrodynamic applications. These findings provide new insights into the behaviour of tandem foils and may inform the design of next-generation WIG vehicles, hydrofoil vessels, tandem sails, and other systems where foil interactions are significant.

Keywords: Ground effect, lift, drag, interference effect, RANS, tandem foil

1. Introduction

Ground effect (GE) and finite depth phenomena have been the subject of extensive research, with the primary goal of understanding the complex flow dynamics and hydrodynamic responses of lifting surfaces when operating in close proximity to a boundary such as the ground or water surface. This comprehensive study investigates how the GE influences vehicle performance, where the reduced distance to the surface enhances the lift and modifies the overall aero/hydrodynamic behaviour [1-3]. The flow characteristics and hydrodynamic behaviour in GE (IGE) are distinct from those encountered in freestream flow conditions, necessitating further analysis.

Address for Correspondence: Mehmet Delikan, İstanbul Technical University Faculty of Naval Architecture and Marine Sciences, Department of Naval Architecture and Ocean Engineering, İstanbul, Türkiye
E-mail: delikan22@itu.edu.tr
ORCID ID: orcid.org/0009-0009-5244-4731

While conventional aircraft experience GE during critical phases such as take-off and landing, wing-in-ground (WIG) vehicles are specifically designed to leverage this phenomenon to achieve higher lift-to-drag ratios by flying just above the water surface. These vehicles combines the naval architecture and aerospace engineering principles, enabling them to operate efficiently in a hover-like state over the water [4]. By bridging the operational gap between ships and airplanes, WIG vehicles offer a compelling transportation solution that combines the fuel efficiency and higher cruising speeds of aircraft with the stability and endurance of marine vessels [5]. Compared to conventional craft, WIG vehicles exhibit enhanced aerodynamic and hydrodynamic efficiency, which contributes to significant improvements in fuel economy and operational speed. This combination of benefits has sparked growing international interest and investment in the development of WIG technology, driving further research into the aerodynamics and hydrodynamics of GE to optimize vehicle design and performance.

1.1. Literature Survey

The impact of ground proximity on aero/hydrodynamic performance has been explored experimentally since the early 20th century. One of the earliest methods was the fixed ground simulation, where the ground is represented by a stationary surface, such as a wind tunnel bottom [6]. A second approach, the image method, involves using two identical wind tunnel models, one inverted, to create a symmetrical flow about an imaginary ground plane [7]. However, this method mainly simulates inviscid GE and presents challenges in achieving perfect symmetry. The most precise technique for modelling GE is the moving belt system, which simulates the relative motion of the ground by running a belt at freestream velocity, though it comes with practical difficulties, including vibrations and belt flatness [8]. Werle's work in the 1960's further highlighted the significant differences between these methods, particularly in flow separation and vortex behaviour under various conditions [9].

GE phenomena are generally classified into two categories: two-dimensional (2D) chord-dominated GE and three-dimensional (3D) span-dominated GE [10]. In 2D chord-dominated GE, the proximity to the ground increases the pressure on the lower surface (pressure side) of the foil, resulting in a significant enhancement in lift, an improved performance of foil. In contrast, for 3D wings, GE causes the outward displacement of wingtip vortices, which reduces downwash and consequently lowers induced drag.

Previous studies have extensively explored 2D GE at low to moderate angles of attack (AoA). For instance, Hsiun and Chen [11] investigated a NACA 4412 foil at 5° and 10° AoA and found that lift increased as ground clearance (H) decreased, peaking at specific height-to-chord ratios. However, at very close distances, lift dropped sharply due to recirculation zones and increased adverse pressure near the ground. Similarly, Chun [12] used numerical simulations on the NACA 4412 and Clark Y foils, demonstrating that lift and pitching moment predictions were similar for both static and moving ground models, though drag was lower in the fixed-ground setup.

An investigation was performed to assess the aerodynamic behaviour of the NACA 4412 foil under GE, using a moving belt apparatus to replicate ground proximity. Flow data were gathered via particle image velocimetry at a Reynolds number (Re) of 3×10^5, with AoA ranging from 0° to 10°. Findings indicated that at smaller AoA ($\alpha\leq4°$), the lift coefficient (C_L) tended to decrease as the foil neared the simulated ground. This outcome was attributed to an elevated pressure along the lower surface and a reduction in suction on the upper surface. Conversely, at larger angles ($\alpha\geq6°$), an increase in C_L was observed due to substantial pressure buildup beneath the foil. Furthermore, drag coefficient (C_D) values were noted to rise with reduced H, particularly at higher angles, influenced by the specific contour of the passage between the foil and the ground, which impacted the lift force [13].

An investigation was undertaken to study the WIG effect using a Tyrrell 026 Formula 1 car's front wing in a wind tunnel. Their findings demonstrated that aerodynamic performance was highly dependent on ride height, with significant changes noted as the wing moved closer to the ground. In particular, they noted the onset of boundary layer separation near the trailing edge, which became more pronounced at reduced ride heights. The reduction in aerodynamic force was attributed to a balance between minimal downforce loss from flow separation and increased velocity on the lower surface at reduced ride heights [14].

Qu et al. [15], conducted a numerical study examining the aerodynamic properties of NACA 4412 foil IGE while simulating a moving ground surface at a Re of $6\text{x}10^6$. The investigation encompassed a wide range of AoA, from -4° to 20°, and H ratios (H/c) ranging from 0.05 to infinity. They found that, for AoA between 2° and 12°, the C_L initially decreased as the foil approached the ground, followed by a significant increase in lift at very close proximity (region I). This behaviour was linked to a reduction in the effective AoA, which raised the pressure on the suction side while lowering it on the lower surface. Additionally, a blockage effect caused further pressure buildup on the lower surface. In region II, the reduction in effective AoA had a stronger influence than the blockage effect, causing a decrease in lift. However, as the foil transitioned into region I, the blockage

effect became more pronounced, taking precedence and resulting in a substantial lift increase. Moreover, at elevated AoA, the transition from region II to region I occurred at smaller Hs. For AoA greater than 12°, airflow separation became more pronounced, expanding in response to the increasingly adverse pressure gradient as H decreased. This condition caused a notable increase in pressure on the upper surface (suction side), resulting in reduced lift across all Hs, with C_L decreasing as the foil close to the ground. Stall conditions were observed to occur earlier and more abruptly at lower H/c values due to the intensified adverse pressure gradient close to the ground.

Hayashi and Endo [16], reported an increase in the separation region during their experimental and numerical investigations of the wake behind a NACA 4412 foil operating at 15° AoA (post-stall) and a Re of $3.2x10^5$. Their findings indicated that as the foil approached the ground, the wake region expanded significantly, resulting in an earlier onset of stalling compared to scenarios out of ground effect (OGE). These observations aligned with those noted by Qu et al. [15].

As previously mentioned, the ground conditions in experimental setups can vary considerably. In addition to various experimental studies examining these ground types, numerous numerical analyses have been conducted. A study by Barber et al. [17] explored four distinct ground conditions to assess their effects on aerodynamic performance. Beyond the traditional stationary and moving ground conditions, the researchers also investigated two additional models: A "slip" boundary condition, defined by the absence of shear stress at the boundary, and an "image" ground condition, which involved simulating two identical bodies reflected across a symmetry plane to mimic the effects of the ground.

In addition to viscous flow solvers, previous research has examined GEs on foils operating above free surfaces. While many studies have investigated various ground conditions, including fixed and moving boundaries, a notable body of work focuses specifically on foils above free surfaces [18-23]. Iterative numerical methods have been extensively employed to evaluate the performance of foils and wings in close proximity to free surfaces. The Iterative Boundary Element Method (IBEM) is used to predict the hydrodynamic behavior of WIG effect vehicles flying above a free water surface. Originally designed for submerged hydrofoils, IBEM has been extended to account for WIG-specific conditions. The method divides the problem into two parts: One for the wing and wake effects, and one for the free surface. These parts interact iteratively using Green's theorem. Both components are modeled with panels that have dipole and source distributions, enabling analysis of how factors like Froude number, H, and wing geometry affect the lift and drag forces on WIG vehicles [18]. Bal [19] adapted a method initially designed for submerged cavitating hydrofoils to analyse 2D foils and 3D wings above free water surfaces. Their perturbation potential formulation effectively resolved interactions between the foil and the free surface, yielding strong agreement with experimental C_L data for NACA 0004 and NACA 0015 foils across various Froude numbers and clearance ratios. The study highlighted that higher Froude numbers generally enhanced aerodynamic loading on the foil, with free surface effects, particularly wave patterns, becoming more pronounced at reduced clearance ratios.

Building on this foundation, Dogrul and Bal [20] applied an IBEM combined with a finite volume approach to predict the aerodynamic performance of a 3D wing steadily moving above a free water surface. Their findings showed that the free surface significantly increased aero/hydrodynamic loading compared to unbounded flow, particularly at smaller clearance ratios. They also noted the development of a Kelvin wave pattern on the free surface, with an increase in the wing aspect ratio further causing an increase in loading. These insights suggest that unsteady and viscous effects are critical factors in the aerodynamic design of wings and foils operating near free surfaces, warranting further investigation in future work.

Kinaci and Bal [21] utilized a similar approach to investigate a foil near the ground under inviscid flow conditions, comparing solid ground and free surface scenarios. Their validation against experimental data revealed that lift and C_Ds increased with decreasing clearance ratios due to GEs, while wave heights and wavelengths on the free surface grew larger with higher Froude numbers, emphasizing the importance of these effects in design considerations.

Bal [22] presents an analytical model using a lumped vortex element to calculate the C_L of a 2D flat plate flying over a free water surface. The study focuses on high-speed conditions and applies potential flow theory, satisfying boundary conditions both on the plate and the water surface. Results show that the C_L is significantly affected by the Froude number, clearance height, and AoA, influencing wave formation on the surface. This work provides insights into the performance of WIG marine vehicles, such as racing boats.

Bal [23] presents an analytical solution for the hydrodynamics of a 2D flat plate moving beneath a free surface in finite depth water. Using a lumped vortex element and the method of images, the study calculates the C_L and analyses wave deformation. Key findings show that lower Froude numbers increase lift, while higher Froude numbers and shallower depths result in larger wave heights. The study also highlights the influence of finite depth and AoA on the hydrodynamic performance of submerged bodies, providing valuable insights for marine applications.

Despite the extensive body of research on GE in single-wing configurations, relatively little attention has been devoted to tandem wing setups, particularly in the context of GE. The benefits of tandem wing designs have been recognized since the early stages of aviation development. From Prandtl's early biplane theory to advanced Navier-Stokes simulations, studies have consistently highlighted the aerodynamic advantages of tandem wings. However, it is important to note that there is no universally applicable design criterion for all tandem configurations. Each configuration demands a comprehensive analysis that considers the mission requirements, specific size and weight limitations, as well as the desired aerodynamic characteristics.

Tandem foil configurations hold significant promise for enhancing the performance of both sail and hydrofoil vessels by improving lift, reducing drag, and optimizing overall hydrodynamic efficiency. In sail vessels, tandem foils can be employed to distribute aerodynamic loads more evenly, improving stability and increasing sailing speed. By adjusting the lift-to-drag ratio, these configurations help mitigate leeway drift and reduce the risk of capsizing, particularly under varying wind and sea conditions. This has been particularly relevant in competitive yacht racing, where optimizing the aerodynamic efficiency of the vessel is paramount. For instance, in America's Cup racing yachts, tandem or multi-element foils have been explored to enhance upwind and downwind performance through reduced induced drag and improved load distribution [24].

In hydrofoil vessels, tandem foil configurations are beneficial for maintaining stability and efficiency at high speeds. By lifting the hull out of the water, hydrofoil boats reduce drag and increase fuel efficiency. Tandem foils improve lift distribution between the fore and aft foils, which leads to enhanced stability, particularly in rough sea conditions, while reducing wave-making resistance [25,26]. This configuration also helps mitigate issues related to cavitation at high speeds, a common problem in hydrofoil systems. As a result, tandem hydrofoil arrangements are increasingly being considered for high-speed ferries and naval applications where efficiency, stability, and safety are critical [27].

The potential of tandem foils to contribute to green shipping initiatives is also being explored, as these configurations can significantly enhance energy efficiency in marine vessels. By reducing drag and improving lift, tandem foils offer an opportunity to design faster and more sustainable ships, aligning with current environmental objectives. These benefits, along with future developments in adaptive or morphing foil technologies, position tandem foil configurations as a promising area of continued research and innovation in marine technology [28].

Khan and Mueller [29] examined the influence of the vortical wake generated by a finite-span canard on the aerodynamic performance of a low Re wing, emphasizing that the position of the canard's tip vortex and wake significantly alters wing performance. Building on prior research, Rokhsaz [30] employed vortex panel methods to analyse tandem configurations of NACA 62-215 and NACA 0012 foils, confirming the aerodynamic benefits identified by earlier studies while elucidating the underlying mechanisms of drag reduction.

Fanjoy and Dorney [31] explored the aerodynamic characteristics of tandem foil systems, observing that reducing the horizontal distance between foils leads to an increase in drag on the aft foil, while the fore foil exhibits improved aero/hydrodynamic efficiency through an expanded drag bucket and a higher performance. In a comprehensive investigation of turbulent flow around tandem foils in a T-configuration, Faure et al. [32] focused on high AoA at moderate Re. Their study detailed how the wake generated by the fore foil affects the aerodynamic performance of the aft foil, including changes in C_L and vortex dynamics. Their statistical analysis of the velocity field revealed critical features such as wake velocity deficits, recirculation zones, and turbulence intensities that play a key role in describing the flow characteristics within the detached region.

Further advancing this field, Yin et al. [33] conducted a study on the aero/hydrodynamic performance of tandem NACA 0012 foils operating in IGE case at ultra-low Re (Re=500). Their findings demonstrated that tandem configurations provide superior aerodynamic performance compared to single foil setups, especially when vertical distance between foils is positive. Their analysis also highlighted the influence of horizontal and vertical distance between foils, and ride height (H/c) on flow dynamics, including the formation of laminar separation bubbles. These bubbles, observed within the wake of the fore foil, were found to induce oscillations in the flow, ultimately impacting the lift and drag of the aft foil and offering insights into optimizing aerodynamic efficiency.

1.2. Objectives of the Study

Despite considerable research on the aero/hydrodynamics of 2D foils, there is a critical gap in understanding the flow characteristics of tandem foils operating IGE, particularly at moderate Re. This study seeks to address this gap by conducting a comprehensive numerical investigation of NACA 4412 foils arranged in a tandem configuration near a moving ground. By fixing the AoA at $\alpha=4°$ for both foils, the study eliminates decalage effects, allowing for a focused analysis at $Re=3\times10^5$.

This extensive study methodically examines the impact of horizontal and vertical spacing between foils, as well as ride

height (H/c), on the lift, drag, and overall performance of the tandem configuration. The findings are benchmarked against baseline data from isolated foil cases to assess the impact of foil-to-foil interactions. In addition, the aero/hydrodynamic performance of the tandem foils is evaluated under both GE and non-GE conditions. This approach provides valuable insights into how ground proximity affects aero/hydrodynamic efficiency and the overall aero/hydrodynamic behaviour of the tandem system.

2. Model Geometries and Parameter Definition

This study examines the aero/hydrodynamic efficiency of NACA 4412 foils in tandem arrangements, considering both IGE and OGE conditions. The relative positioning of the foils is defined by three key parameters: horizontal separation (S), vertical offset (G), and H. S is characterized as the distance from the trailing edge of the front foil to the leading edge of the rear foil. G indicates the vertical distance between the trailing edges of both foils, with positive values signifying that the front foil is positioned higher than the rear foil. H is defined as the vertical distance from the trailing edge of the front foil to the ground surface. These parameters, as illustrated in Figure 1, are critical in analysing the interaction effects and overall hydrodynamic efficiency of the tandem foil configuration.

NACA 0012 foil was validated in case of OGE in the thesis [34], and the NACA 4412 foil was similarly validated in the conference paper [35]. As these validations are documented in those works, they are not repeated here. Upon successful validation, twenty tandem configurations are investigated, encompassing scenarios both with and without the influence of GE. Table 1 provides an overview of the parameters for these configurations.

3. Solution Method

The unsteady, incompressible Reynolds-averaged Navier-Stokes (RANS) equations were employed in the analyses. In Cartesian tensor form, these equations can be represented as follows:

$$\frac{\partial U_i}{\partial x_i} = 0 \tag{1}$$

$$\rho \frac{\partial (U_i)}{\partial t} + \rho \frac{\partial (U_J U_i)}{x_j} = -\frac{\partial P}{\partial x_i} + \frac{\partial}{\partial x_j}\left(\mu S_{ij} - \overline{\rho \acute{U}_i \acute{U}_j}\right) \tag{2}$$

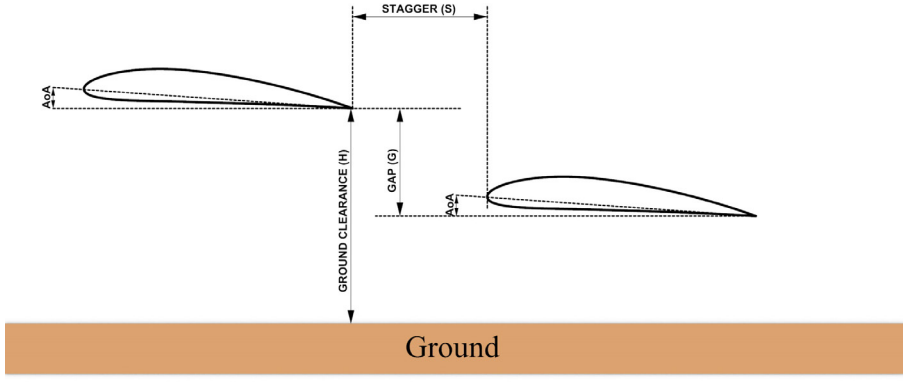

Figure 1. Geometric configuration of foils in tandem case.

AoA: Angle of attack

Table 1. Test cases.

Case no	Stagger distance (S)	Gap (G)	Ground clearance (H)	Case no	Stagger distance (S)	Gap (G)	Ground clearance (H)
Case 1	0.25c	-0.4c	0.4c	Case 11	0.25c	-0.4c	-
Case 2	0.50c	-0.4c	0.4c	Case 12	0.50c	-0.4c	-
Case 3	1c	-0.4c	0.4c	Case 13	1c	-0.4c	-
Case 4	2c	-0.4c	0.4c	Case 14	2c	-0.4c	-
Case 5	4c	-0.4c	0.4c	Case 15	4c	-0.4c	-
Case 6	0.25c	0.4c	0.8c	Case 16	0.25c	0.4c	-
Case 7	0.50c	0.4c	0.8c	Case 17	0.50c	0.4c	-
Case 8	1c	0.4c	0.8c	Case 18	1c	0.4c	-
Case 9	2c	0.4c	0.8c	Case 19	2c	0.4c	-
Case 10	4c	0.4c	0.8c	Case 20	4c	0.4c	-

in this context ρ, μ, U, P and Ú refer to the fluid's density, dynamic viscosity, average velocity, mean static pressure, and fluctuating velocity, respectively. S_{ij} term in equation (2), corresponds to the mean strain rate tensor, while the expression $-\rho\overline{Ú_I Ú_j}$ accounts for the stresses resulting from turbulent fluctuations, known as Reynolds stresses, with the overbar signifying a time-averaged value. ANSYS Fluent was utilized for the simulations, with the k-ω Shear Stress Transport (SST) turbulence model [36], grounded in the Boussinesq approximation [37]. This approach incorporates two extra transport equations for turbulence kinetic energy and its dissipation to capture the effects of Reynolds stresses in the RANS equations.

The RANS and turbulence transport equations were solved using the finite volume method with the coupled algorithm for pressure-velocity coupling. A second-order upwind scheme was used for flow simulation, while PRESTO and first-order implicit schemes were applied for pressure and transient formulations, respectively. In unsteady simulations, the time step was set for a CFL number of 1. Convergence was confirmed with scaled residuals below 10^{-5}, and the stability of aero/hydrodynamic forces was monitored. Simulation accuracy was verified through mesh quality assessments and comparison with experimental data.

4. Verification and Validation of NACA 4412 IGE

2D flow characteristics around the foil were analysed through computational fluid dynamics (CFD) simulations performed using ANSYS fluent. The unsteady RANS equations were resolved with a coupled solver, under the assumption of constant fluid density. Convergence was successfully attained across all simulations, with residuals decreased to a threshold of 10^5, thereby validating the accuracy and reliability of the computational solutions.

The simulations implemented the k-ω SST turbulence model with gamma transition model. The computational domain was specifically designed to extend 20 chord lengths (20c) in front of the foil's leading edge, 25 chord lengths behind the trailing edge, and to a vertical extent of 20c.

GE aerodynamics were investigated through both steady and unsteady CFD simulations, building upon insights from prior studies [38,39]. The results indicated that unsteady simulations, while requiring greater computational resources, produced findings that exhibited closer alignment with experimental data. In contrast, steady simulations demonstrated higher error margins, particularly regarding the C_D across all ride height (H/c) ratios. The ride height (H) refers to the vertical distance between the trailing edge of the foil and the ground surface, consistent with established conventions in the literature [40]. This alignment facilitates meaningful comparisons with existing research.

A second-order upwind scheme was employed for the unsteady flow simulations surrounding the foil, with the exception of pressure and transient formulations, which utilized the PRESTO! scheme and a first-order implicit method, respectively. The time step size for the unsteady simulations was selected to ensure CFL number of 1. The accuracy of the simulations was rigorously validated through comprehensive assessments of mesh quality, grid independence, and by comparing the resulting lift and drag against established experimental data.

Due to the significant impact of ground proximity on flow pattern around the foil, a refined mesh was implemented in the area between the foil and the ground to accurately resolve the steep flow gradients. The foil surface was subjected to no-slip boundary conditions, ensuring an average y+ value close to 1 for precise boundary layer resolution.

The conditions applied for the simulation were specified as: left side was set as a velocity inlet, the right side served as a pressure outlet, and the upper boundary was configured as a symmetry plane. The moving ground condition, aligned with the incoming flow velocity, was implemented to effectively replicate the GE. This configuration resulted in a chord Re of $3x10^5$, aligning with the experimental conditions reported by Ahmed et al. [13].

The validation of the simulations for the baseline NACA 4412 foil IGE was achieved by comparing the computed C_L and C_D with experimental wind tunnel data from Ahmed et al. [13]. A GCI study was conducted at a 4-degree AoA and a ride height (H/c) was 0.15, employing the k-ω SST turbulence model with the gamma transition model. To assess numerical uncertainty and determine an appropriate grid resolution, a GCI analysis was performed following Roache's methodology. Three distinct grids with varying levels of refinement were employed: the coarsest mesh (G), the moderately refined mesh (H), and the finest mesh (I), as shown in Figure 2. The results presented in Table 2 indicate that the relative errors (e_L) and (e_D) and GCI values between mesh configurations H and I were sufficiently low, confirming grid independence. Based on this analysis, mesh H was selected for all subsequent validation runs to ensure a balance between computational efficiency and numerical accuracy.

The simulations employed the k-ω SST model, with a gamma transition, to evaluate the performance characteristics of the NACA 4412 foil. A systematic comparison was conducted against experimental data collected at heights ranging from 15% to 80% of the chord length above a moving ground surface, all while maintaining a constant AoA of 4 degrees. Figure 3 displays a comparison of the calculated C_L and C_D with the measured values. The k-ω SST model

demonstrated a remarkable accuracy in predicting both lift and drag, effectively capturing the dynamics associated with the laminar-turbulent transition. Additionally, the surface pressure distributions confirmed the model's effectiveness in accurately predicting the occurrence of a laminar separation bubble on the upper surface of the foil, consistent with the results described by Ahmed et al. [13]. The numerical results align with those presented by Qu et al. [15], providing further validation of the laminar separation bubble's presence. Consequently, the findings of this study are consistent with the established literature, underscoring the robustness of the modelling approach adopted.

Figure 3 displays a comparative analysis between the findings of this study and the corresponding experimental results. Although employing high-fidelity CFD techniques, such as detached-eddy simulation or large-eddy simulation, could potentially mitigate these discrepancies, computational resource limitations constrain the breadth of cases explored within this investigation. The average-C_D error recorded within the range of 0.15 to 0.8 H/c is 3.5%, while the average C_L error for the same interval is 4.9%. The strong correlation observed in Figures 3 and 4 between the numerical outcomes and Ahmed's experimental findings validates the effectiveness of the employed methodology, underscoring its adequacy for accurately capturing the relevant flow dynamics.

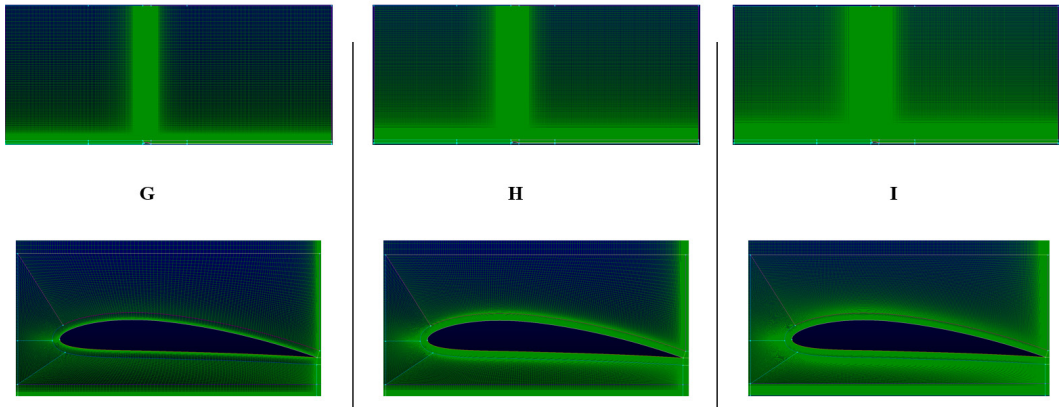

Figure 2. Grid refinement for NACA 4412 in ground effect.

Table 2. Grid convergence index results for NACA 4412 in ground effect.

Case	Mesh name	C_L	C_D	e_L	e_D	GCI_L	GCI_D	Average y+	Cell number
NACA4412 AoA=4° H/c=0.15	**G**	0.894	0.01145	-	-	-	-	0.89	248860
	H	0.929	0.00992	0.03753	0.15389	0.01073	0.04401	0.94	500498
	I	0.935	0.00975	0.00694	0.01754	0.00198	0.00276	0.87	1006946

AoA: Angle of attack, C_D: Drag coefficient, C_L: Lift coefficient, GCI: Grid convergence index, G: Coarsest mesh, H: Moderately refined mesh, I: Finest mesh

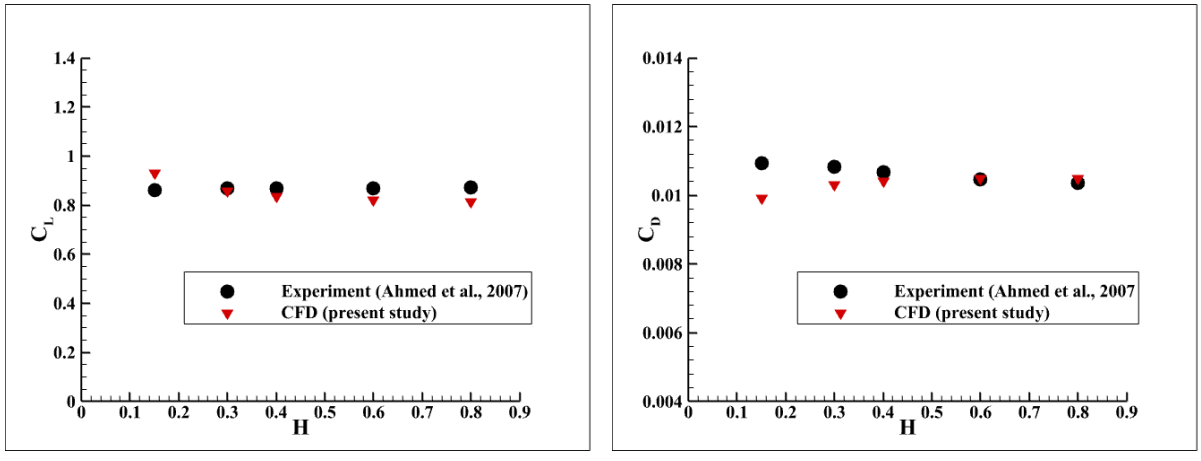

Figure 3. Comparison of results of present study and experimental results.

CFD: Computational fluid dynamic, C_D: Drag coefficient, C_L: Lift coefficient

5. Computational Domain and Mesh Configuration for Tandem Foils

In the simulations of two tandem foils, both assumed to have a NACA 4412 profile, the AoA is fixed at 4°, indicating no decalage between the foils. The Re is maintained constant at $3x10^5$.

5.1. Tandem Foils OGE Case

Figure 5 illustrates the computational domain and mesh arrangement for the tandem foils operating in an unbounded flow domain. The domain covers 20 chord lengths (20c) starting from the front foil's leading edge to the left side and extends 25c from the aft foil's trailing edge to the right side, with a total height of 40c. Velocity inlet conditions are applied on the left, top, and bottom sides, while a pressure outlet is set on the right side.

5.2. Tandem Foils in IGE Case

In the analysis of tandem foils operating within GE, the NACA 4412 foil profile is employed with a fixed AoA of 4° and a Re of 3×10^5. The computational domain for these simulations is depicted in Figure 6. Here, the inlet boundary is positioned 20c from the leading edge of the fore foil, while the outlet boundary is 25c from the trailing edge of the aft foil, with the total domain height set at 20c. The boundary conditions implemented include a velocity inlet on the left side, a symmetry condition along the upper boundary, and a pressure outlet on the right. The bottom boundary, which simulates the ground, is modelled as a moving wall to effectively reduce the formation of a viscous boundary layer. Furthermore, the surface of the foil, characterized by the NACA 4412 profile, is treated as a no-slip wall, achieving an average y+ value close to 1.

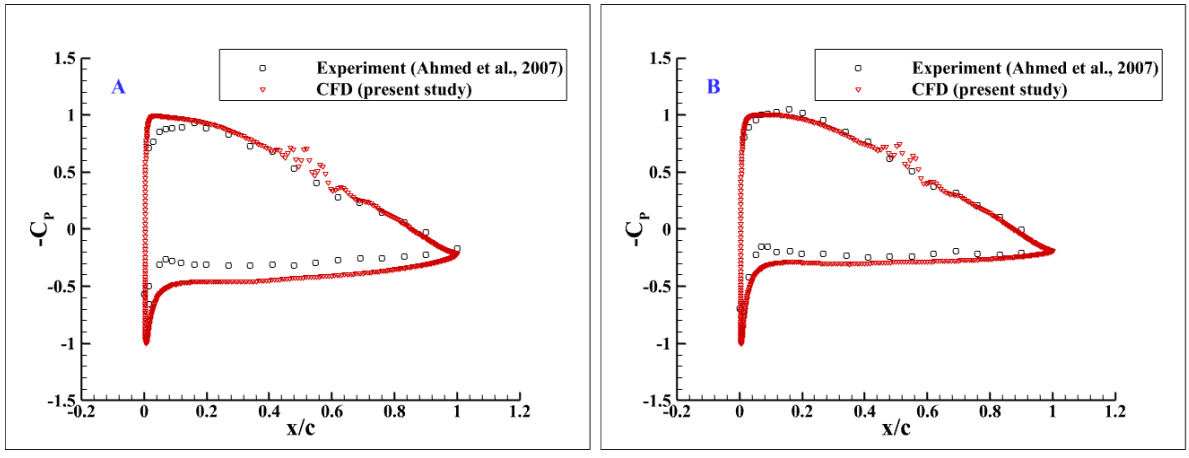

Figure 4. Pressure distribution comparison. **A)** H/c=0.15, **B)** H/c=0.40.

CFD: Computational fluid dynamic, C_p: Pressure coefficient

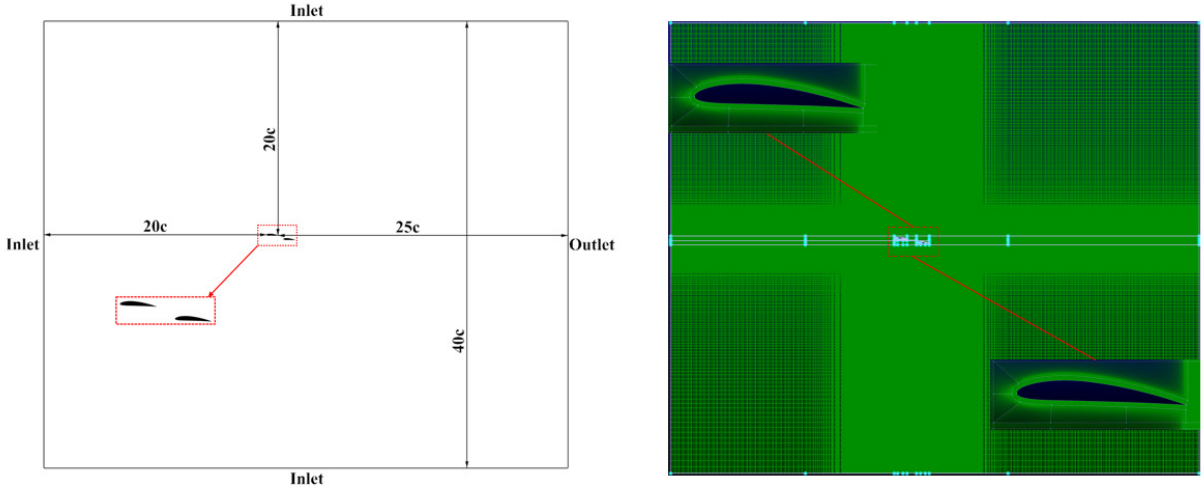

Figure 5. Computational domain and mesh configuration for the tandem foils outside of ground effect.

5.3. Meshing and Simulation Parameters for Tandem Cases

Figures 5 and 6 illustrate the computational mesh, featuring increased resolution near the foil surfaces to accurately capture velocity gradients, as well as additional refinement in the wake region to enhance flow field resolution. The mesh configuration supports the numerical approaches outlined in section 4, ensuring effective turbulence modelling and numerical stability. These figures provide a visual representation of the computational framework that facilitates the detailed analysis of the flow characteristics around the foils.

6. Results and Discussion

The comprehensive findings of present study are organized into three sub-sections to enhance clarity and depth of analysis. Section 6.1 presents a comprehensive examination of a single foil operating IGE, emphasizing the intricate flow dynamics associated with this configuration. Section 6.2 offers an in-depth analysis of selected scenarios involving the foil operating OGE, providing a meticulous assessment of the flow characteristics in these instances. Finally, section 6.3 focuses on a thorough evaluation of specific cases within GE, similarly detailing the related flow behaviour and aero/hydrodynamic performance.

6.1. Single Foil IGE

The analysis of the NACA 4412 foil IGE was conducted at a 4-degree AoA across a range of ride heights. As demonstrated in previous study [15], the pressure distribution of the airflow between the lower surface of the foil and the ground is critical in influencing the WIG effect. Figure 7 illustrates the airflow passage, which can be classified as either convergent or divergent. In instances of a convergent passage, where the inlet area (A1) exceeds the outlet area (A2), the airflow accelerates, leading to a decrease in static pressure, in accordance with the venturi effect. This phenomenon underscores the importance of flow geometry in optimizing the aerodynamic performance of foils operating IGE.

Figures 8 and 9 show the distribution of the pressure coefficient (C_p) for the NACA 4412 foil at different H/c. Figure 8 offers a graphical representation of the C_p along the foil, while Figure 9 presents a contour plot that delineates the pressure distribution over the foil's surface.

As illustrated in Figure 8, when the foil moves closer to the ground, the stagnation point shifts toward the trailing edge, increasing pressure on the lower surface. Notably, pressure on the suction surface, particularly close to the leading edge, rises due to GE. The maximum negative pressure occurs near this leading edge area on the suction side, where the slower airflow reduces suction pressure.

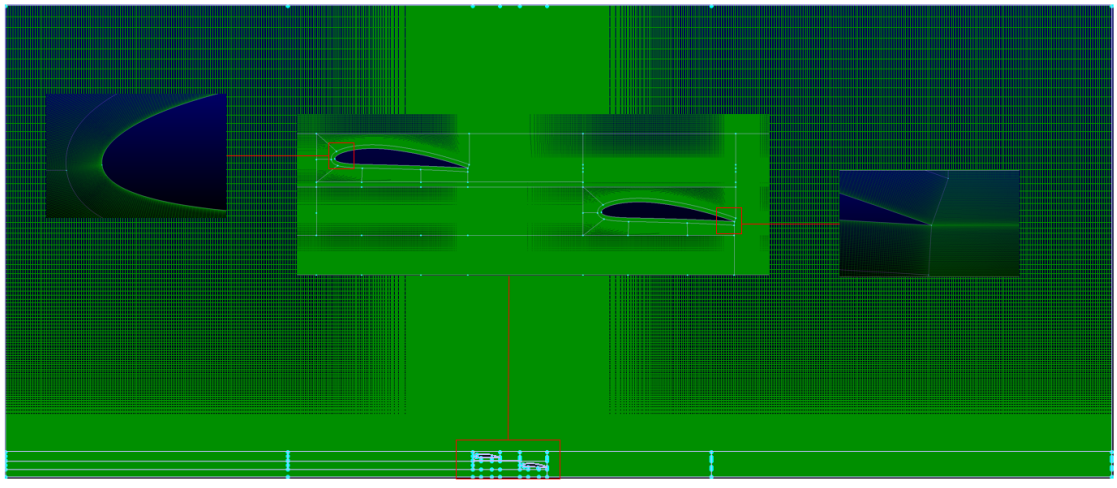

Figure 6. Computational mesh for tandem NACA 4412 foils in ground effect.

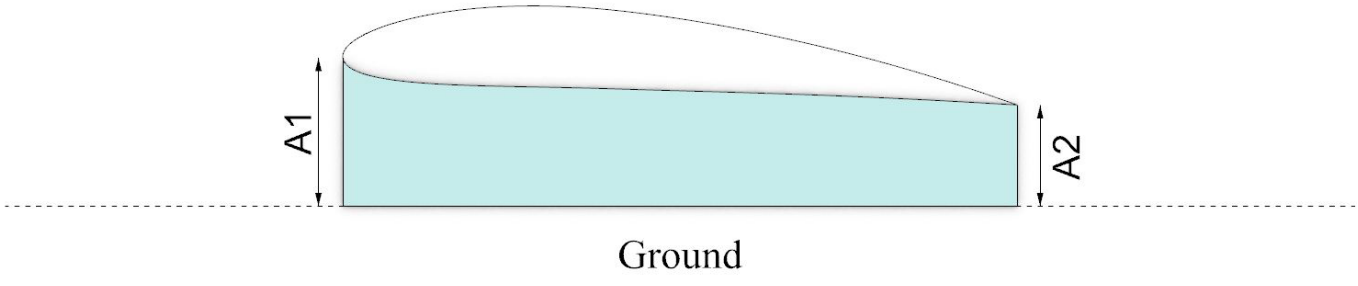

Figure 7. A convergent-divergent flow passage in proximity to the ground.

Conversely, the highest pressure on the lower surface is found near the leading edge at the stagnation point, where an increase in flow velocity corresponds to a reduction in static pressure. The fluid velocity beneath the foil significantly diminishes as it nears the ground. When the ride height (H/c) is reduced, the C_P correspondingly increased, indicating that the rise in static pressure beneath the foil consistently surpasses the reduction in suction pressure above it. This observation suggests that GE positively influences the C_L. Furthermore, the position of the positive pressure peak, corresponding to the stagnation point, shifts toward the trailing edge at reduced ride heights, a phenomenon that can

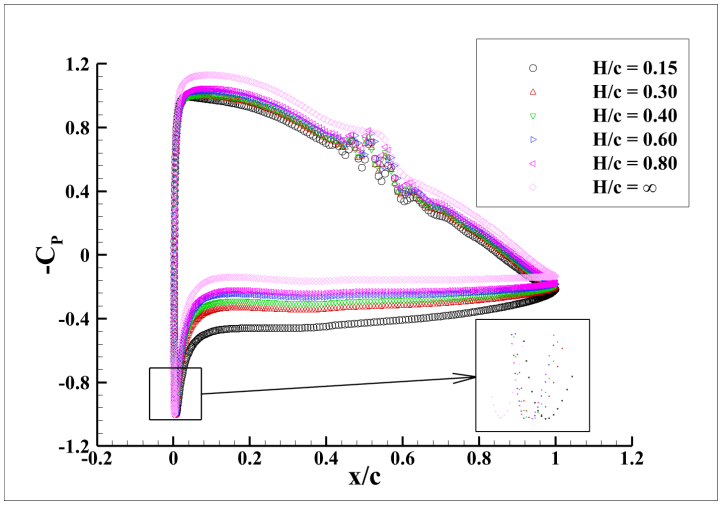

Figure 8. Pressure distribution across varying ground clearances.

C_P: Pressure coefficient

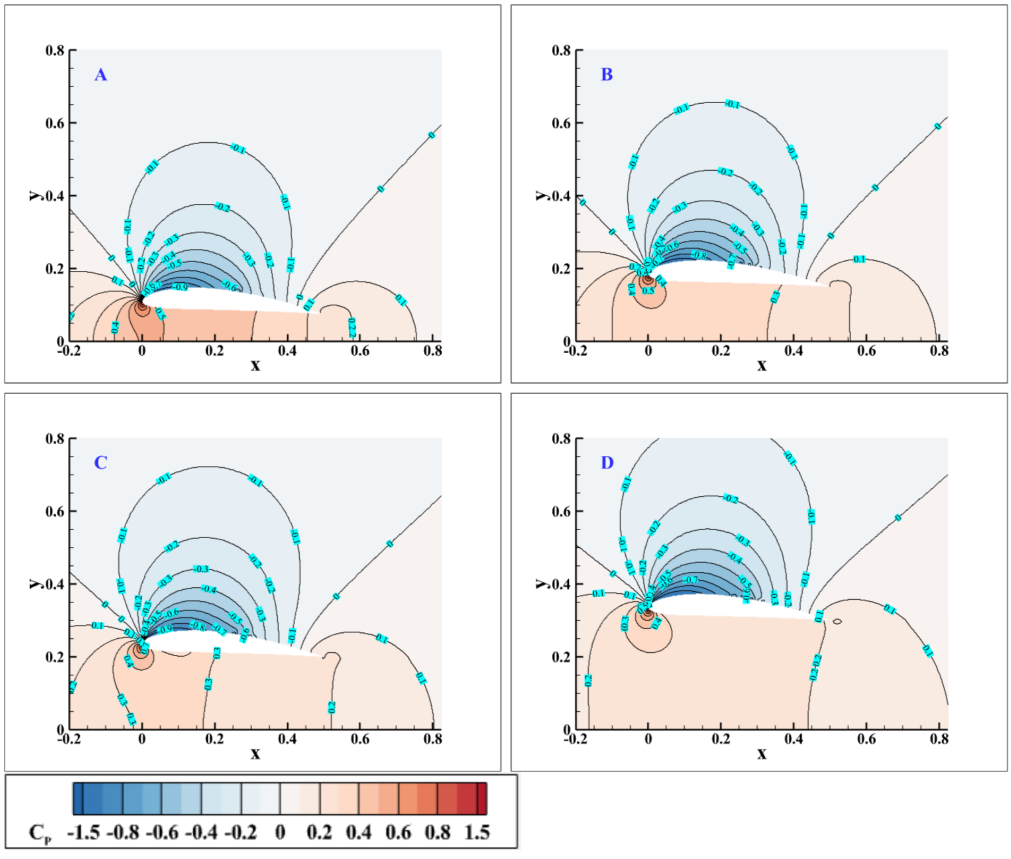

Figure 9. Comparison of pressure distribution for different ground clearances; **A)** H/c=0.15, **B)** H/c=0.30, **C)** H/c=0.40, **D)** H/c=0.60.

C_P: Pressure coefficient

be ascribed to the characteristics of the convergent-divergent flow region illustrated in Figure 7.

In the present study, Figure 8 reveals that the separation bubble is evident on the upper surface of the foil across all tested H/c, as well as in conditions where the foil is OGE. Notably, the bubble's position relative to the chord length (x/c) remains unchanged, irrespective of the proximity to the ground. As previously discussed, the decrease in airflow velocity over the upper surface of the foil, induced by GE, results in a reduction in suction pressure. This observation suggests that GE adversely affects the suction pressure on the upper surface of the foil. Consequently, the C_P curve for the suction side experiences a downward shift, while the position of the separation bubble remains unaffected.

As the H diminishes, the convergence-to-divergence ratio increases, resulting in more pronounced airflow acceleration or deceleration. This effect is illustrated in the pressure distribution for varying height-to-chord (H/c) ratios, as depicted in Figure 8. Furthermore, the influence of ground proximity on pressure distribution is clearly represented in Figure 9.

Figure 10 demonstrates the existence of a separation bubble on the upper surface of the foil, a physical phenomenon that aligns with the observations made by Winslow et al. [41]. Their research indicated that for AoA ranging from 0° to 8°, the separation bubble migrates from the trailing edge toward the leading edge, effectively altering the transition point from laminar to turbulent flow. However, this migration was not observed at higher Res, specifically at $Re=1\times10^6$.

Figure 11 illustrates the ratio of velocity magnitude to freestream velocity around a NACA 4412 foil operating at an AoA of 4° for various ride heights (H/c). As the foil approaches the ground, a notable decrease in velocity magnitude on its lower surface occurs, leading to a rise in static pressure beneath the foil.

The pressure distribution on the suction side of the foil exhibits a maximum negative pressure near the leading edge. This reduction in air velocity across the upper surface of the foil, attributed to GE, corresponds with a decrease in suction pressure. It appears that GE adversely impacts the suction pressure experienced by the foil. Conversely, the maximum static pressure on the lower surface of the foil is noted near the leading edge, especially at the stagnation point, where increases in flow velocity result in decreases in static pressure.

Furthermore, the fluid velocity close to ground significantly decreases beneath the foil. It is noteworthy that with a reduction in ride height (H/c), the C_P tends to increase. The augmentation of static pressure below the foil consistently exceeds the reduction in suction pressure above its upper surface. Thus, proximity to the ground is anticipated to positively contribute to the lift force C_L generated by the foil. Additionally, the proximity of the foil to the ground results in an expansion of the wake region, which suggests an increase in the pressure drag component.

To elucidate the observed reduction in streamline deflection within GE, we employ the mirror-image model. This theoretical framework introduces an imaginary foil positioned below the ground, effectively mirroring the real foil situated above. The real foil exhibits clockwise circulation, denoted as -Γ, while the image foil displays anticlockwise circulation, represented as Γ, as illustrated in Figure 12. The circulation generated by the image foil induces downwash in the upstream region and upwash in the downstream region, thereby significantly influencing the behaviour of streamlines in proximity to the ground [42].

IGE flow fields, the proximity of the ground and the induced flows from the image foil lead to a predominantly straight configuration of streamlines until they approach the foil closely. This phenomenon results in a more localized region of streamline deflection in comparison to the expansive

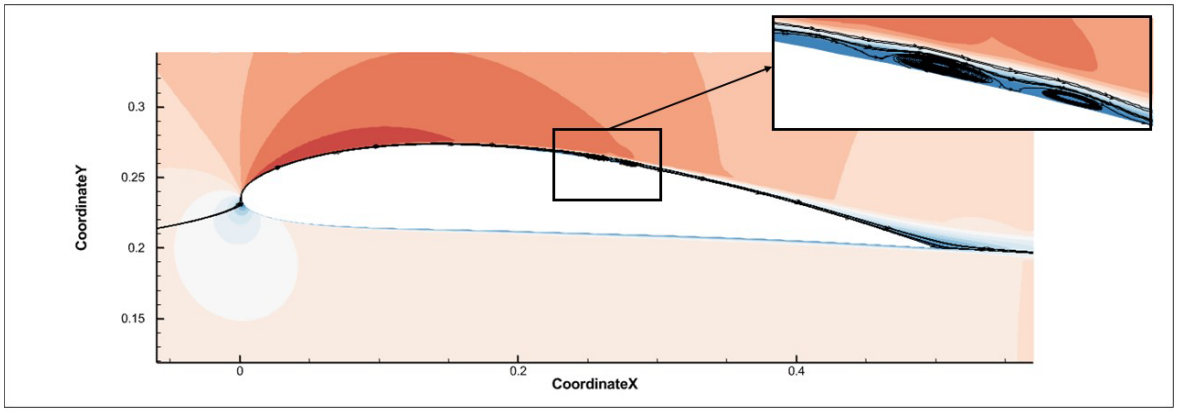

Figure 10. Separation bubble observed at a reynolds number of $3x10^5$. The red arrow indicates the location of the separation bubble.

deflection region observed in unbounded flow case. As the clearance decreases, the point at which streamline deflection commences migrates closer to the foil, further concentrating this deflection zone. Thus, the mirror-image model offers a robust theoretical framework for elucidating the observed reduction in streamline deflection underground-effect conditions.

For AoA that generate positive lift, the presence of the foil induces an upward deflection of the surrounding streamlines, as depicted in Figure 13. In an unbounded flow field, this region of deflection extends substantially from the inlet to the outlet. However, in a ground-effect flow field, the deflection is markedly more constrained, occurring primarily in the immediate vicinity of the foil. In this scenario, the streamlines tend to remain predominantly straight until they near the leading edge of the foil [15].

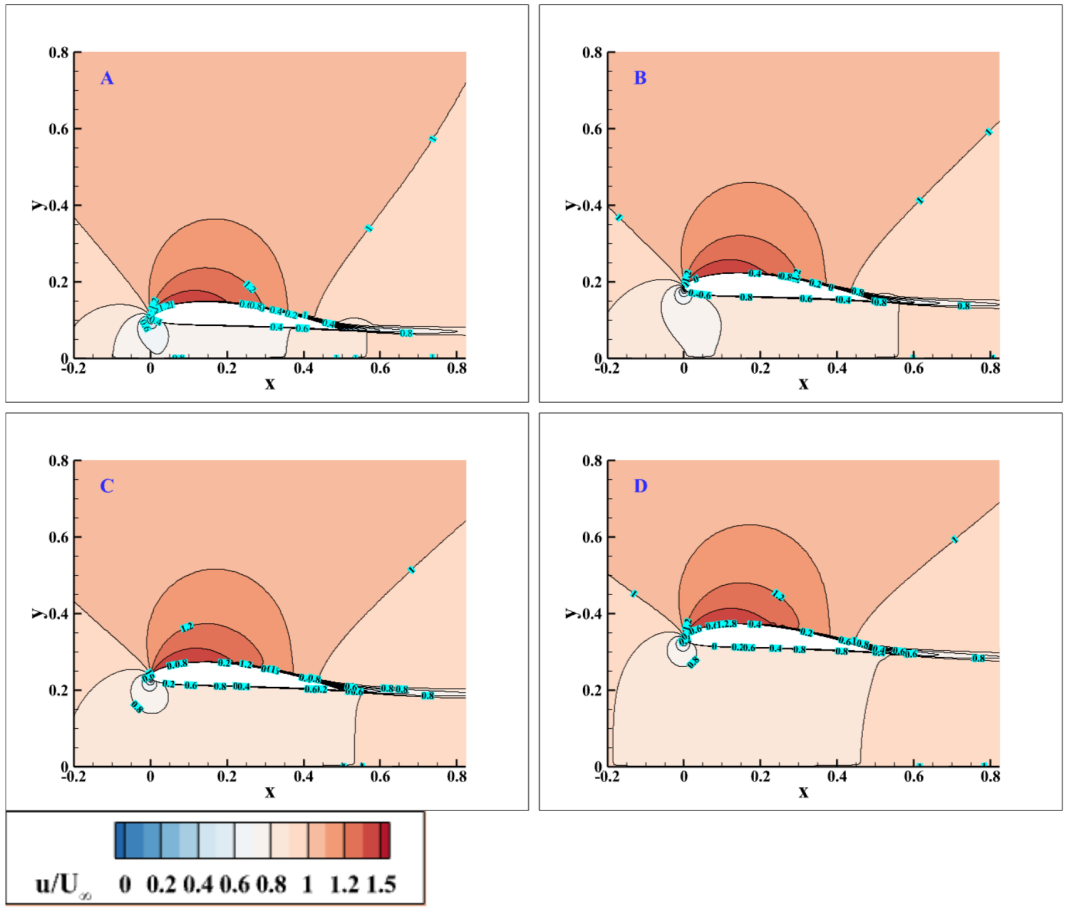

Figure 11. Velocity magnitude to freestream velocity around NACA 4412 foil. **A)** H/c=0.15, **B)** H/c=0.30, **C)** H/c=0.40, **D)** H/c=0.60.

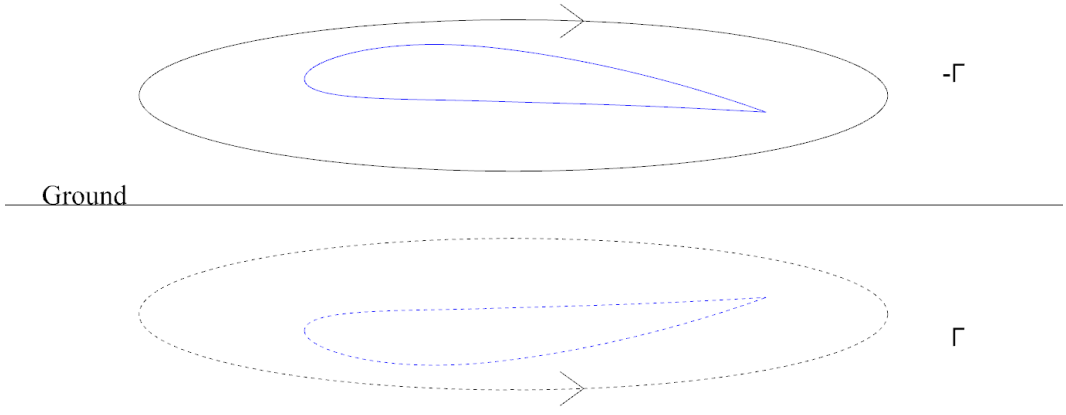

Figure 12. Mirror-image model.

When a foil operates IGE, the surrounding airflow characteristics undergo substantial changes compared to those in an unbounded flow environment. For a foil generating positive lift, the induced circulation leads to a notable upward deflection of adjacent streamlines. In an unbounded flow condition, this deflection region is extensive, significantly influencing the overall airflow dynamics from the inlet to the outlet.

In the context of GE, the reduced upward deflection of streamlines leads to two critical outcomes: A decrease in the effective AoA and an obstruction of airflow beneath the foil.

6.2. Tandem Cases

6.2.1. Reference data: Foil only configuration without interaction effects

To assess the interaction effects between the tandem foils, the results obtained from the tandem configuration were compared against baseline data derived from the analysis of each foil. This comparison effectively eliminates any interaction influences and establishes a benchmark for reference. The baseline data were generated through simulations of each foil in isolation, maintaining consistent conditions for Re and AoA in both IGE and OGE scenarios. The reference values for the C_L and C_D of the leading foil were obtained from simulations conducted at the same H used in the tandem configuration. Likewise, the reference data for the aft foil were derived from isolated simulations at the same clearance distance. The average reference values for the tandem configuration were calculated by taking the mean of the coefficients from the individual foil analyses. Convergence was confirmed when fluctuations in lift and C_D fell below $1x10^{-5}$, indicating negligible numerical dispersion.

In the reference framework, the lift and drag aero/hydrodynamic coefficients are expressed as:

$$C_{l(reference)} = \frac{C_{l(individual\ fore)} + C_{l(invididual\ aft)}}{2} \quad (3)$$

$$C_{d(reference)} = \frac{C_{d(individual\ fore)} + C_{d(invididual\ aft)}}{2} \quad (4)$$

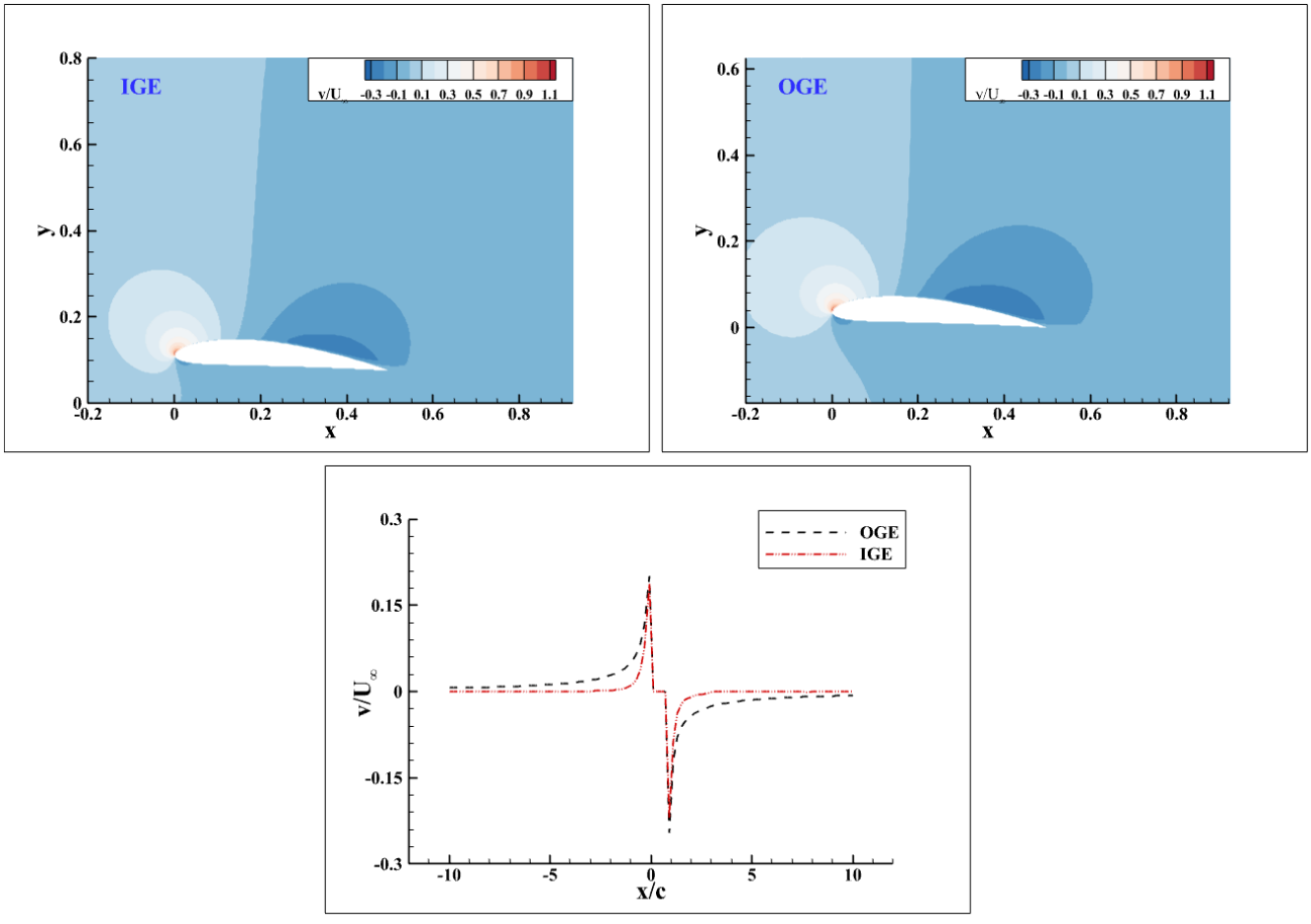

Figure 13. Non-dimensional velocity contour plot (top), non-dimensional velocity distribution along x-axis (bottom).

In the tandem framework, the lift and drag aero/hydrodynamic coefficients are expressed as:

$$C_{l(tandem)} = \frac{C_{l(fore)} + C_{l(aft)}}{2} \quad (5)$$

$$C_{d(tandem)} = \frac{C_{d(fore)} + C_{d(aft)}}{2} \quad (6)$$

6.2.2. Effect of gap distance in OGE case

Presented in Figure 14, the pressure distributions for the isolated foil, the fore foil in the negative gap configuration (case 13) (see Table 1), and the positive gap configuration (case 18) at a constant stagger distance (S) of (S=1c) reveal that the presence of the aft foil significantly influences the pressure distribution on the fore foil. Specifically, the stagnation point on the fore foil shifts slightly towards the trailing edge compared to the isolated foil scenario. This shift is evident in both tandem configurations; however, the distinction between the negative and positive gap cases is subtle. Notably, case 18 exhibits a more pronounced shift in the location of the minimum C_P relative to case 13, which can be attributed to the more favourable aero/hydrodynamic positioning of the fore foil in the positive gap configuration.

The impact of gap distance on the aero/hydrodynamic performance of tandem foils in the absence of GE has been rigorously analysed by examining the C_L and C_D as functions of S, as depicted in Figure 15. These figures illustrate the variations in C_L and C_D, along with the performance of foils, for gap distances between -0.4c and 0.4c.

Figure 15 shows the C_L of both the aft and fore foils under negative and positive gap conditions. Notably, the C_L of the aft foil consistently remains lower than the corresponding reference value across both gap configurations, exhibiting minimal sensitivity to variations in gap distance. Conversely, the fore foil demonstrates an increased C_L relative to the reference, with a more pronounced enhancement observed in positive gap conditions, indicating a heightened sensitivity of the fore foil lift to positive gaps.

The presence of the fore foil significantly influences the aerodynamic performance of the aft foil. Notably, the stagnation points on the aft foil shift towards the leading edge compared to the isolated foil scenario, resulting in a reduced maximum suction coefficient C_P value. This shift indicates a decrease in the effective AoA for the aft foil, despite both foils maintaining the same geometric AoA. Furthermore, the area under the C_P curve for the aft foil is smaller than that of the isolated foil, which can be attributed to the momentum deficit created by the wake of the fore foil.

In contrast, the lift curve for the fore foil demonstrates an upward trend with an increase in gap distance, while its C_D remains relatively stable, suggesting enhanced aerodynamic efficiency under these conditions. The lift and C_D for the aft foil, however, exhibit minimal changes with variations in gap distance, indicating a lower sensitivity to adjustments in gap spacing.

The tandem configuration exhibits a diminished lift-to-drag ratio in both positive and negative gap conditions relative to the reference values. This reduction arises from the fore foil's enhanced lift and decreased drag, which are counterbalanced by a reduction in lift and an increase in drag for the aft foil. As a result, the beneficial aero/hydrodynamic performance of the fore foil is partially offset by the suboptimal performance of the aft foil, leading to an overall decline in the aero/hydrodynamic efficiency of the tandem system, regardless of the gap condition.

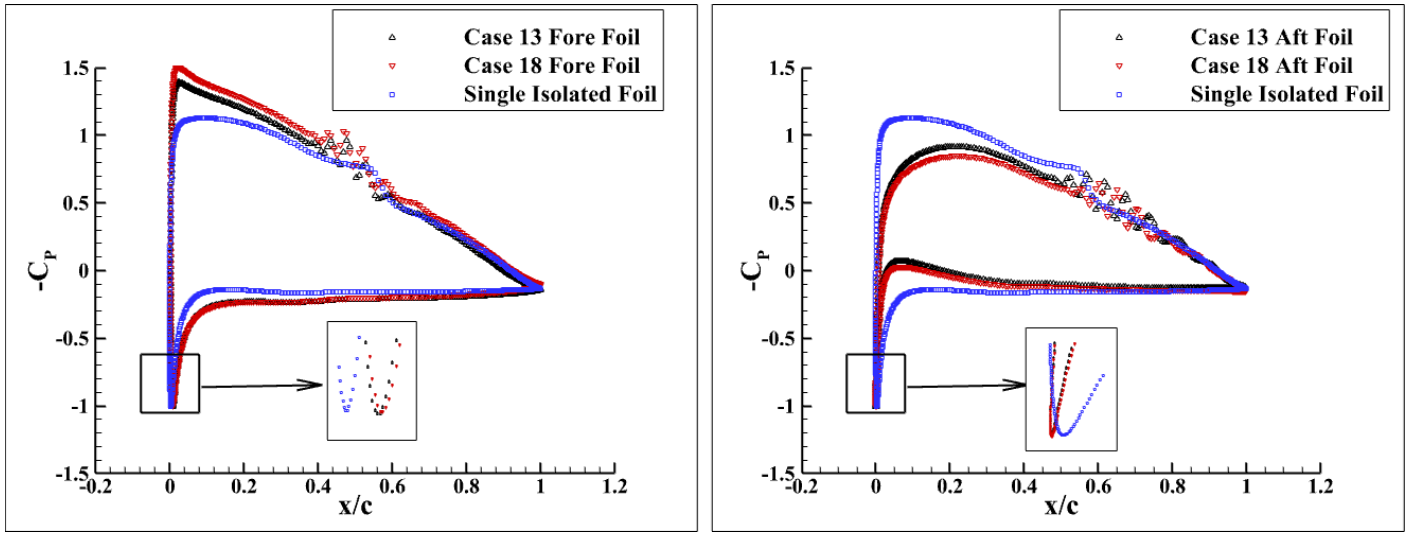

Figure 14. Influence of stagnation point variations on pressure distributions.

C_P: Pressure coefficient

6.2.3. Effect of S in OGE case

This section examines the effect of S on the aero/hydrodynamic characteristics of the system under both positive and negative gap configurations. As previously established, the results indicate a consistent reduction in performance across both gap scenarios. Figures 15 illustrates the variations in C_L and C_D, as well as the performance of foil, in relation to S for each gap condition.

As the S increases in both negative and positive gap configurations, a notable trend emerges: the C_L of the fore foil decreases, whereas the C_L of the aft foil increases. This phenomenon is indicative of diminishing interference effects between the foils as the S increases. Notably, the reduction in lift for the fore foil is more pronounced in the positive gap configuration, suggesting that the favourable interference effects enhancing lift in this configuration are less effective at greater S.

As the S between the foils increases, the C_D of the fore foil rises, while that of the aft foil decreases. Despite the reduction in drag on the aft foil and the corresponding increase on the fore foil, the overall mean C_D for the tandem configuration remains slightly elevated compared to the value observed for isolated foils. This trend is likely due to the formation of a high-pressure region between the foils, which generates an upstream force on the fore foil and a downstream force on the aft foil, as depicted in Figure 16.

6.3. Effect of Gap Distance in IGE Case

The influence of gap distance on the aero/hydrodynamic performance of tandem foils in proximity to the ground was analysed by evaluating C_L and C_D as functions of S, as presented in Figure 17. The findings indicate that the lift generated by the aft foil is significantly diminished compared to that of an isolated foil, while concurrently, the aft foil exhibits increased drag relative to the reference values. This

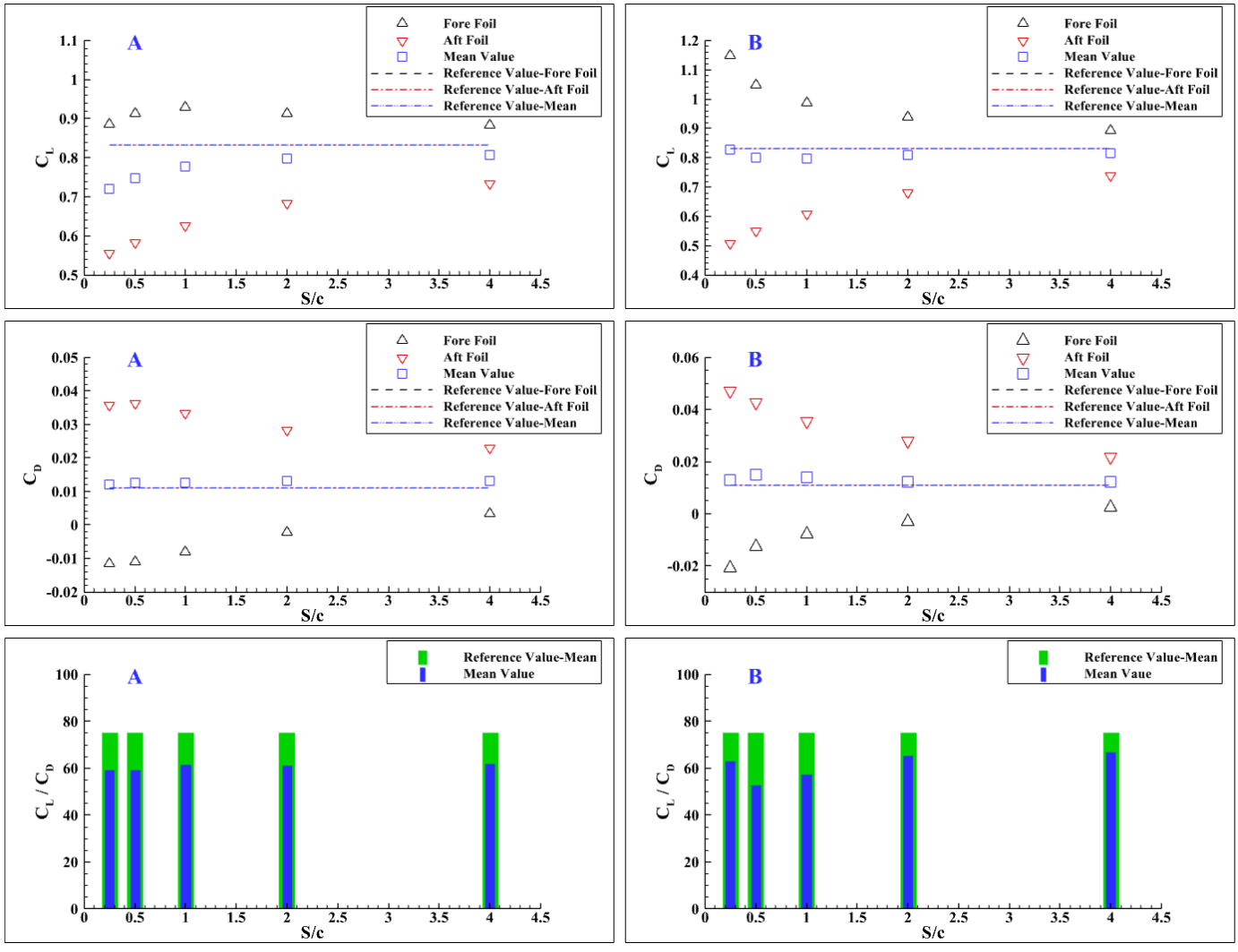

Figure 15. Lift coefficient, drag coefficient, performance of foils in the absence of ground effect. **A)** G=-0.4c, **B)** G=0.4c.

C_D: Drag coefficient, C_L: Lift coefficient

decline in performance is attributed to the aft foil interaction with the intricate wake structures induced by the fore foil, which adversely affects its overall aero/hydrodynamic efficiency.

When the gap height (G) is positive, there is a significant increase in the C_L of the fore foil, despite its greater distance from the ground. This phenomenon can be attributed to the aft foil influence, which causes high pressure on the lower (pressure) side of the fore foil, thereby offsetting the reduction in lift associated with diminished GE. Conversely, in cases where G is negative, the aft foil enhances the pressure on the suction side of the fore foil, as illustrated in Figure 18.

The tandem configuration exhibits improved performance as G increases, primarily driven by the increase in lift on the fore foil and the aft foil ability to mitigate the adverse effects of wake interference near the ground. As a result, with a positive gap, the tandem system achieves significantly higher performance compared to the reference single foil. While a similar trend is observed with negative gap values, the performance enhancement is markedly more pronounced when G is positive.

The fore foil demonstrates a significant reduction in drag across both negative and positive gap configurations, primarily due to the presence of the aft foil, which induces a beneficial interference drag effect. This reduction in overall drag is consistently observed across all tested gap spacings. Moreover, in the positive gap configuration, the lift curve for the fore foil increases while drag remains relatively constant, reflecting improved aero/hydrodynamic efficiency. These findings indicate that a tandem foil configuration can achieve enhanced aero/hydrodynamic performance compared to two isolated foils, particularly when the gap between the foils is positive.

6.3.1. Effect of S in IGE case

As detailed in the preceding section, the aero/hydrodynamic efficiency of tandem foils shows marked improvement when the G between the foils is positive. However, to

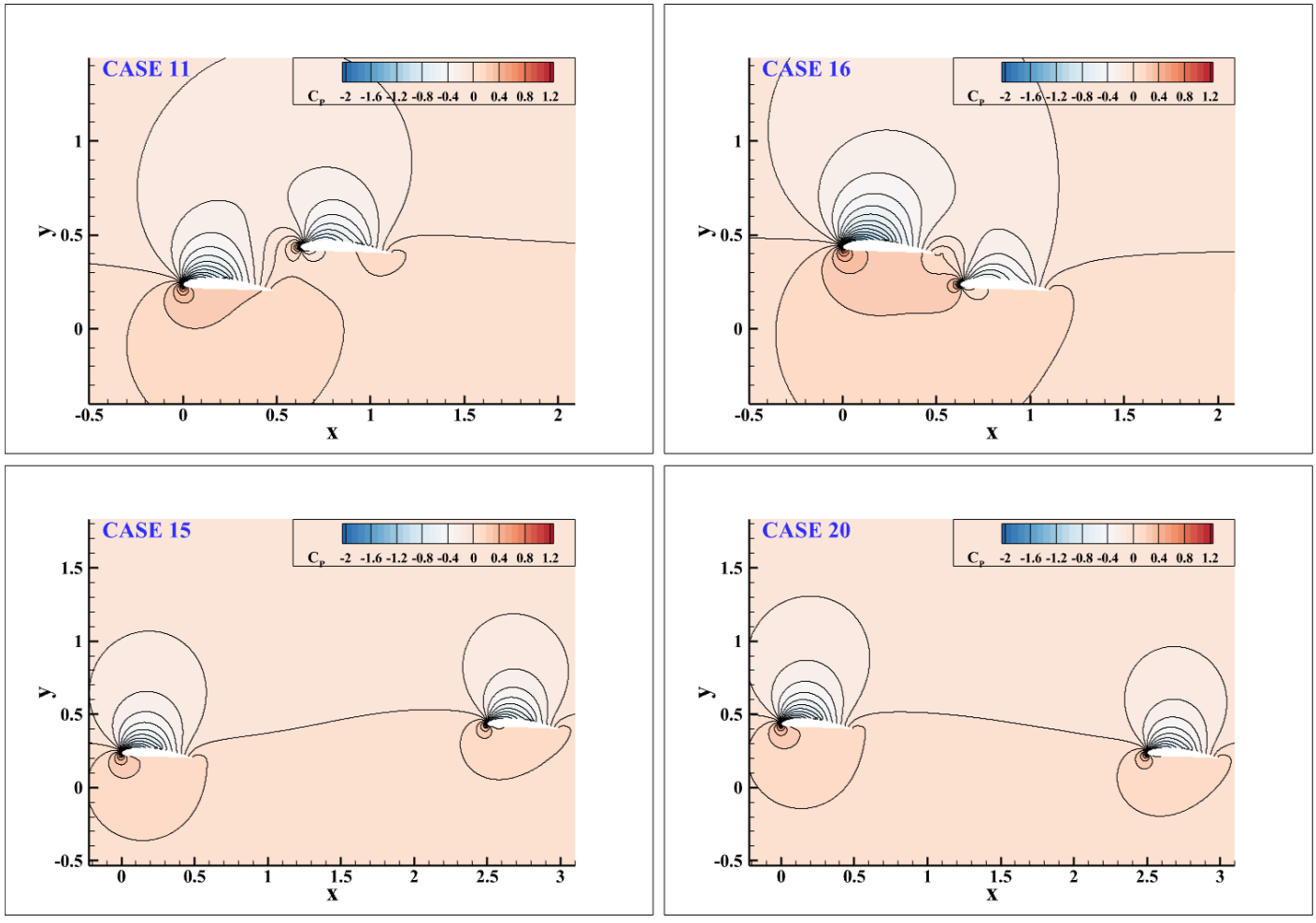

Figure 16. Contours depicting the pressure distribution for the various tested configurations in the absence of ground effect.

C_p: Pressure coefficient

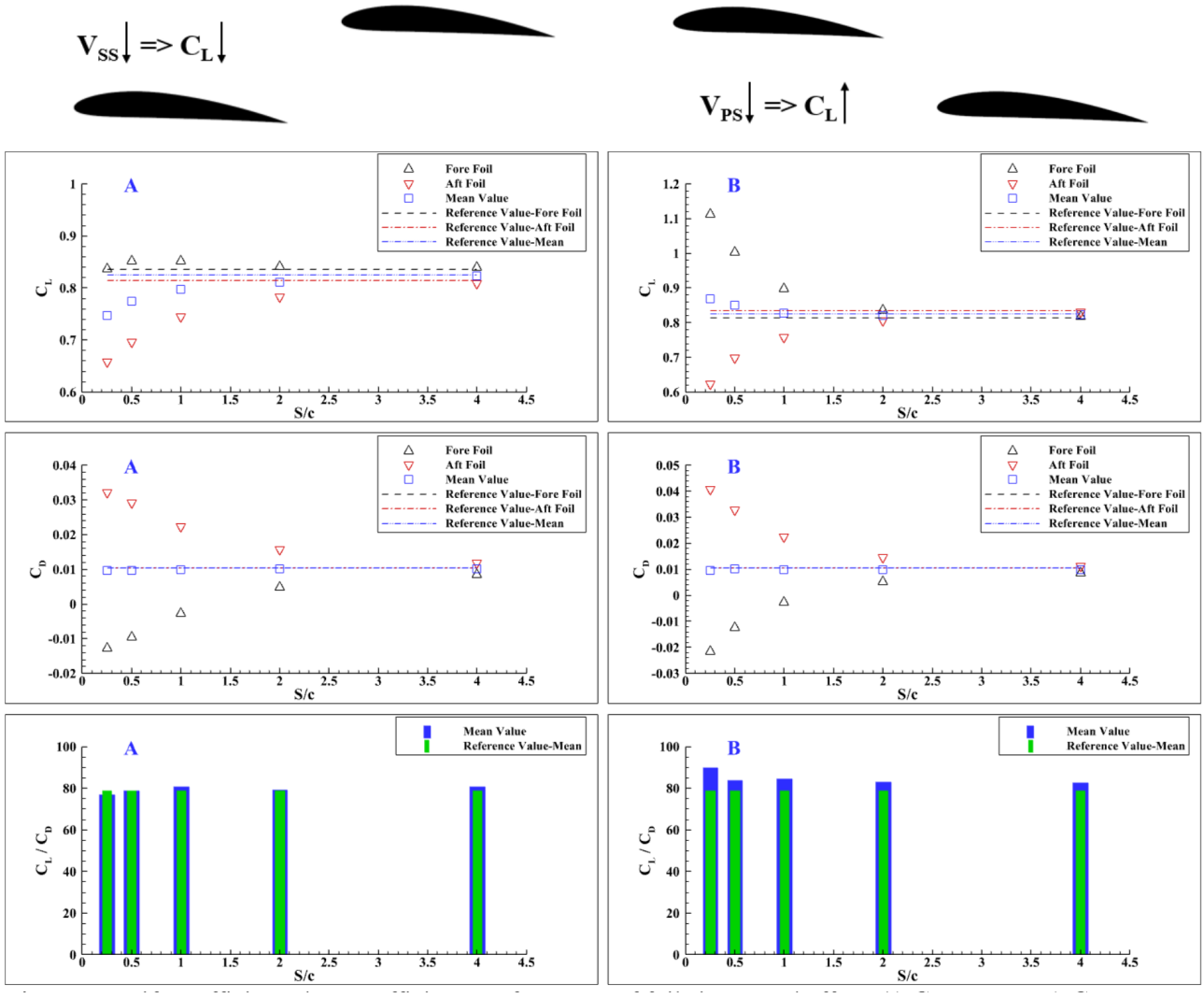

Figure 17. Lift coefficient, drag coefficient, performance of foils in ground effect. **A)** Gap=-0.4c, **B)** Gap=0.4c.

C_D: Drag coefficient, C_L: Lift coefficient

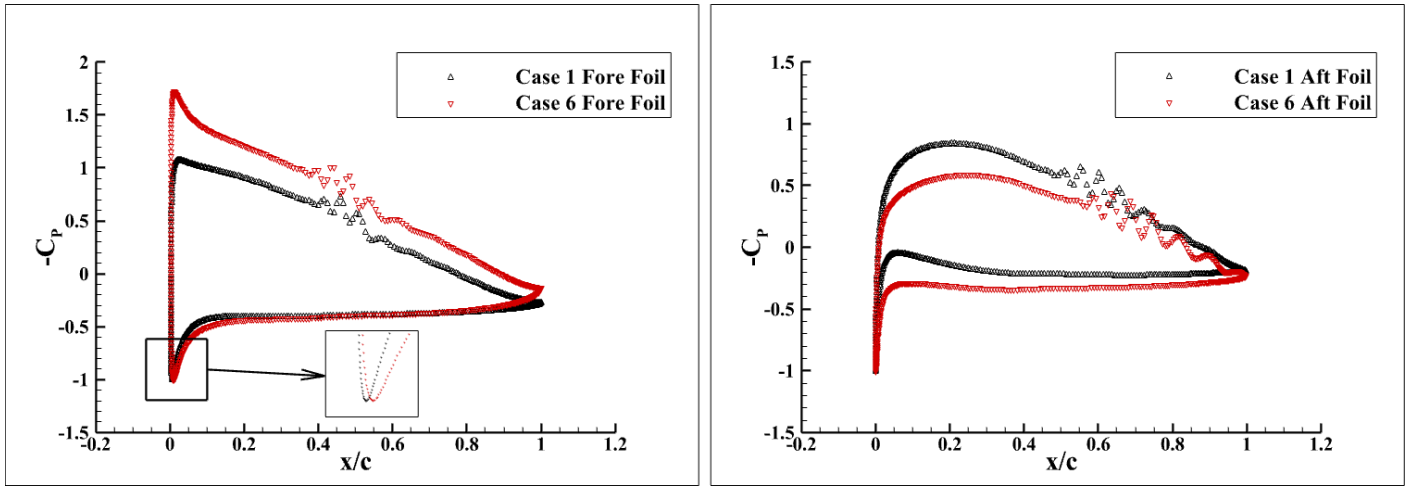

Figure 18. Pressure distributions in tandem configurations with ground effect.

C_P: Pressure coefficient

comprehensively evaluate the influence of S on the system's aero/hydrodynamic behaviour, both positive and negative gap configurations are examined in this section. Figure 17 illustrates the variation in C_L and C_D as functions of S, providing insights into how these parameters evolve with changes in the foil arrangement.

The analysis of drag characteristics reveals that the C_D of the fore foil decreases due to the elevated pressure region created by the aft foil, as demonstrated in Figure 19. Nevertheless, the mean C_D of the tandem system remains comparable to the reference value, indicating a compensatory relationship between the reduced drag on the fore foil and the drag exerted by the aft foil. As the S increases, the C_D of the fore foil exhibits an upward trend, while that of the aft foil decreases. This behaviour can be attributed to the diminishing interference effects between the foils, resulting in a reduced influence of each foil wake and pressure fields on the other as the S increases.

The results of this study are consistent with the trends presented in the experimental work of Biermann and Herrnstein [43], despite the absence of GE in their investigations. Analysing the lift-to-drag ratio (C_L/C_D) reveals that the mean ratio for the tandem system decreases as the S increases, although it remains elevated compared to the reference values for isolated foils. This observation suggests that closer S confer beneficial interference effects, which diminish as the foils are spaced further apart. Notably, at a S of four times the chord length, the aero/hydrodynamic performance metrics of the tandem system converge towards those of a single isolated foil, indicating a significant reduction in aero/hydrodynamic interference between the two foils.

The influence of S on aero/hydrodynamic performance is discernible in both negative and positive gap configurations, with a more significant effect observed in the positive gap scenario as shown Figure 19. Specifically, case 6 illustrates that, despite sharing the same H ratio (H/c=0.80) as in case 9, the fore foil in case 6 generates a higher C_L. This

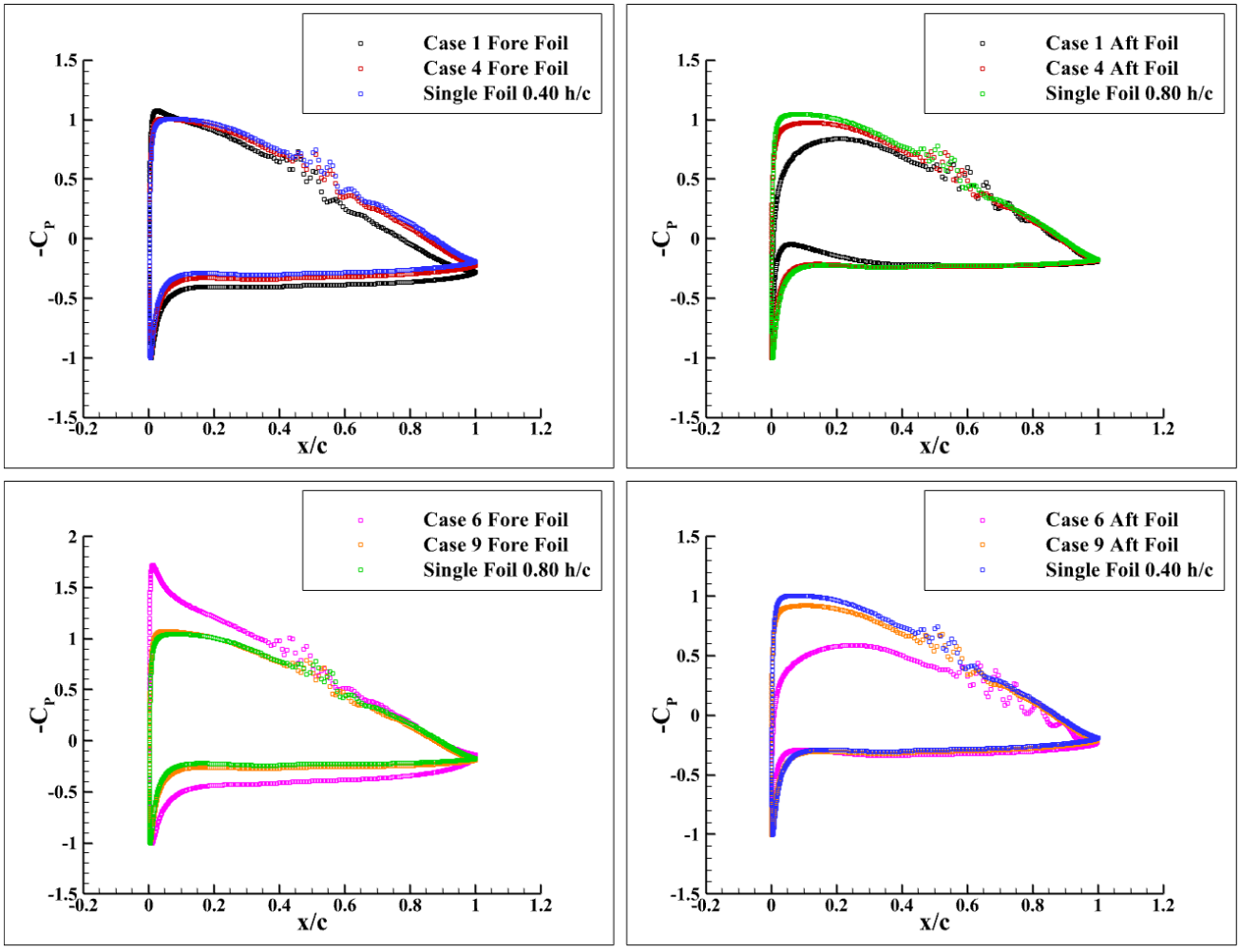

Figure 19. Tested cases pressure distribution in IGE cases.

C_P: Pressure coefficient, IGE: In ground effect

enhancement is attributable to the shorter (S=0.25c in case 6 compared to S=2c in case 9), which facilitates the development of a high-pressure region behind the fore foil due to the presence of the aft foil. As the S increases, this positive pressure region diminishes, signifying a reduction in foil-to-foil interaction effects.

The positive pressure region created by the convergent-divergent zone, alleviates the flow tendency to approach the trailing edge of the fore foil, thereby resulting in a higher suction peak than observed in the isolated case. Furthermore, the positive pressure field generated by the aft foil contributes to a deceleration of the flow on the pressure side of the fore foil, facilitating an increase in pressure in this region. Collectively, these effects enhance the lift production of the fore foil in case 6.

In conclusion, the findings underscore the critical influence of both gap and S on the aero/hydrodynamic performance of tandem foils operating within the GE. Specifically, configurations with positive gaps generally yield enhanced performance. Conversely, increased S diminish the interaction between the foils, leading to performance metrics that approach those of isolated foils (Figure 20).

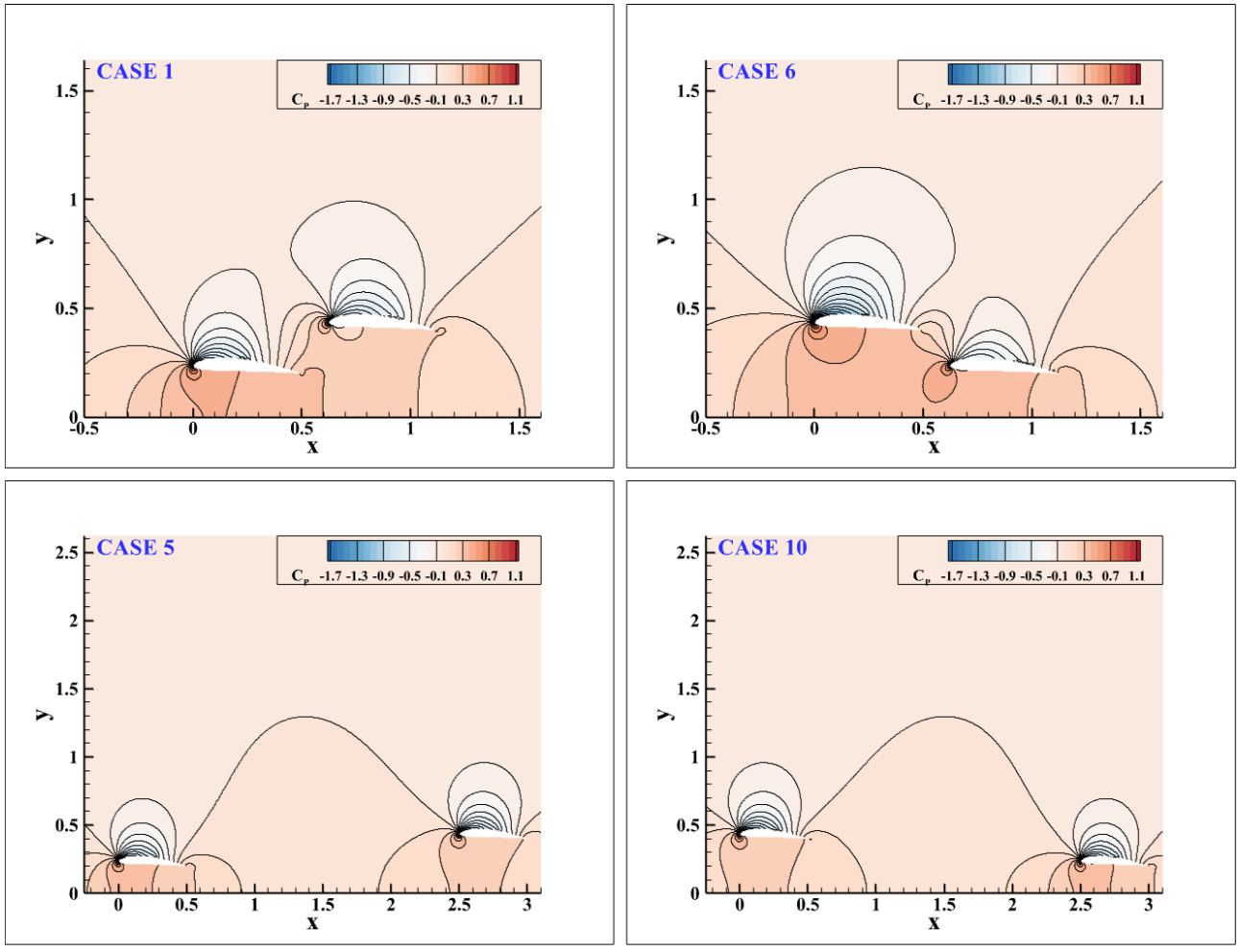

Figure 20. Pressure distribution for various tested configurations in IGE case.

C_P: Pressure coefficient, IGE: In ground effect

7. Conclusion

This original study provides an extensive analysis of the aero/hydrodynamic performance of tandem foils, emphasizing the effects of G, S, and ground. By contrasting tandem configurations with isolated foil cases, the research enhances the understanding of aero/hydrodynamic interactions between the foils. The investigation encompasses a series of simulations and comparative analyses to elucidate how these parameters influence C_L and C_D, as well as the efficiency. The findings yield valuable insights into the effect of these factors on the aero/hydrodynamic efficiency of tandem configurations in both IGE and OGE scenarios.

The main conclusions are as follows:

• It is challenging to assert a single configuration as universally superior without considering specific performance criteria. For instance, achieving maximum range and endurance necessitates an optimal lift-to-drag ratio. In contrast, applications demanding substantial lift forces, regardless of efficiency, or requiring significant drag forces for low-speed flight or short take-off and landing capabilities may prioritize different configurations.

• The tandem system demonstrates a superior lift-to-drag ratio IGE compared to out-of-ground configurations at equivalent stagger and gap distances. While the tandem system OGE exhibits a lower lift-to-drag ratio than the corresponding reference value, the tandem system IGE achieves a higher lift-to-drag ratio in comparison to the reference.

• The aero/hydrodynamic performance of the tandem system is enhanced with a positive G, indicating that an optimal gap can significantly improve system efficiency.

• S significantly affects the performance of the tandem system, primarily due to foil-to-foil interactions that modify the static pressure distribution across the foils.

• In instances of pronounced interference between the foils, the fore foil may experience thrust rather than drag, presenting a considerable advantage for specific applications.

• OGE, the fore foil typically attains a higher C_L than IGE for identical gap and stagger. This variance is attributed to the reduction in the effective AoA induced by GE, which is defined as the angle between the chord line of the foil and the relative airflow impacting the foil. IGE, the proximity of the ground alters the flow field, effectively reducing AoA experienced by the fore foil, resulting in decreased lift. Although both ground and out-of-ground conditions present a notable reduction in lift for the aft foil relative to the reference value, aft foils IGE demonstrate higher C_L compared to their out-of-ground counterparts. This can be explained by the increased pressure on the pressure side of the aft foil due to its closeness to the ground.

In summary, the results indicate that a tandem wing configuration IGE can provide distinct advantages over a single wing design, particularly regarding enhanced aero/hydrodynamic performance under specific conditions.

Footnotes

Authorship Contributions

Concept: M. Delikan, and Ş. Bal, Design: M. Delikan, and Ş. Bal, Data Collection or Processing: M. Delikan, Analysis or Interpretation: M. Delikan, and Ş. Bal, Literature Review: M. Delikan, Writing: M. Delikan, and Ş. Bal.

Conflict of Interest: No conflict of interest was declared by the authors.

Financial Disclosure: The authors declared that this study received no financial support.

9. References

[1] M. R. Ahmed, and S. D. Sharma, "An investigation on the aerodynamics of a symmetrical airfoil in ground effect," *Exp. Therm. Fluid Sci.*, vol. 29, no. 6, pp. 633-647, Jul 2005.

[2] J. Smith, H. Graham, and J. Smith, "The validation of an airfoil in the ground effect regime using 2-D CFD analysis," in *26th AIAA Aerodynamic Measurement Technology and Ground Testing Conference*, Seattle, Washington: American Institute of Aeronautics and Astronautics, Jun 2008.

[3] S. C. Luo, and Y. S. Chen, "Ground effect on flow past a wing with a NACA0015 cross-section," *Experimental Thermal and Fluid Science,* vol. 40, pp. 18-28, Jul 2012.

[4] T. Barber, "Aerodynamic ground effect: a case study of the integration of CFD and experiments," *International Journal of Vehicle Design,* vol. 40, no. 4, pp. 299-316, 2006.

[5] H. Wang, C. J. Teo, B. C. Khoo, and C. J. Goh, "Computational aerodynamics and flight stability of wing-in-ground (WIG) craft," *Procedia Engineering*, vol. 67, pp. 15-24, 2013.

[6] A. F. Zahm, and R. M. Bear, "Ground-plane influence on airplane wings," *Journal of the Franklin Institute,* vol. 191, no. 5, pp. 687-693, May 1921.

[7] K. Park, and J. Lee, "Influence of endplate on aerodynamic characteristics of low-aspect-ratio wing in ground effect," *Journal of Mechanical Science and Technology,* vol. 22, no. 12, pp. 2578-2589, Dec 2008.

[8] A. Klemin, "A belt method of representing the ground," *Journal of the Aeronautical Sciences,* vol. 1, no. 4, pp. 198-199, Oct 1934.

[9] X. Zhang, W. Toet, and J. Zerihan, "Ground effect aerodynamics of race cars," *Appl. Mech. Rev.*, vol. 59, no. 1, pp. 33-49, Jan 2006.

[10] K. V. Rozhdestvensky, "Wing-in-ground effect vehicles," *Progress in Aerospace Sciences,* vol. 42, no. 3, pp. 211-283, May 2006.

[11] C.-M. Hsiun, and C.-K. Chen, "Aerodynamic characteristics of a two-dimensional airfoil with ground effect," *Journal of Aircraft*, vol. 33, no. 2, pp. 386-392, Mar 1996.

[12] H. H. Chun, "Turbulence flow simulation for wings in ground effect with two ground conditions: fixed and moving ground," *International Journal of Maritime Engineering,* vol. 145, pp. 18, 2003.

[13] M. R. Ahmed, T. Takasaki, and Y. Kohama, "Aerodynamics of a NACA4412 Airfoil in Ground Effect," *AIAA J.*, vol. 45, no. 1, pp. 37-47, Jan 2007.

[14] J. Zerihan, and X. Zhang, "Aerodynamics of a single element wing in ground effect," *Journal of Aircraft*, vol. 37, no. 6, pp. 1058-1064, Nov 2000.

[15] Q. Qu, W. Wang, P. Liu, and R. K. Agarwal, "Airfoil aerodynamics in ground effect for wide range of angles of attack," *AIAA Journal*, vol. 53, no. 4, pp. 1048-1061, Apr 2015.

[16] E. Hayashi, and M. Endo, "Measurement of flow fields around an airfoil section with separation," *Transactions of the Japan Society for Aeronautical and Space Sciences,* vol. 21, no. 52, pp. 69-75, 1978.

[17] T. J. Barber, E. Leonardi, and R. D. Archer, "Causes for discrepancies in ground effect analyses," *The Aeronautical Journal,* vol. 106, no. 1066, pp. 653-668, Dec 2002.

[18] S. Bal, "Prediction of hydrodynamic performance of 3-D wig by IBEM," *International Journal of Maritime Engineering*, vol. 160, no. A3, Dec 2021.

[19] S. Bal, "Free surface effects on 2-D airfoils and 3-D wings moving over water," *Ocean Systems Engineering,* vol. 6, no. 3, pp. 245-264, Sep 2016.

[20] A. Dogrul, and S. Bal, "Performance prediction of wings moving above free surface," in *Advances in Boundary Element and Meshless Techniques XVI*, Ankara, Turkey: Middle East Technical University, Ankara, Turkey, 2016, pp. 85-92.

[21] O. K. Kinaci, and S. Bal, "Performance prediction of 2D foils moving above and close to free surface," in *Advances in Boundary Element and Meshless Techniques XVII*, Ankara, Turkey: Middle East Technical University, Ankara, Turkey, 2016, pp. 43-50.

[22] S. Bal, "Lumped vortex element flying over free water surface," *Bulletin of the Technical University of Istanbul,* vol. 55, no. 1, pp. 1-6, 2023.

[23] S. Bal, "Analytic solution for flat-plate under a free surface with finite depth effects," *Ocean Systems Engineering,* vol. 14, no. 3, pp. 301-314, 2024.

[24] J.-B. R. G. Souppez, "*Hydrofoil configurations for sailing superyachts: hydrodynamics, stability, and performance,*" Conference: Design & Construction of Super & Mega YachtsAt: Genoa, Italy, May 2019.

[25] K. I. Matveev, and I. I. Matveev, "Tandem hydrofoil system," *Ocean Engineering*, vol. 28, no. 2, pp. 253-261, Jan 2001.

[26] D. Speranza, S. Papa, C. Pensa, and R. Di Bernardo, "Hydrofoil technology: current applications and future developments for sustainable boating," in *Design Tools and Methods in Industrial Engineering III*, M. Carfagni, R. Furferi, P. Di Stefano, L. Governi, and F. Gherardini, Eds., in Lecture Notes in Mechanical Engineering, Cham: Springer Nature Switzerland, 2024, p. 339-346.

[27] Y. Shang, and J. J. Horrillo, "Numerical simulation and hydrodynamic performance predicting of 2 two-dimensional hydrofoils in tandem configuration," *Journal of Marine Science and Engineering,* vol. 9, no. 5, p. 462, Apr 2021.

[28] O. K. Kinaci, "A numerical parametric study on hydrofoil interaction in tandem," *International Journal of Naval Architecture and Ocean Engineering,* vol. 7, no. 1, pp. 25-40, Jan 2015.

[29] F. A. Khan, and T. J. Mueller, "Tip vortex/airfoil interaction for a low Reynolds number canard/wingconfiguration," *Journal of Aircraft*, vol. 28, no. 3, pp. 181-186, Mar 1991.

[30] K. Rokhsaz, "*Analytical investigation of the aerodynamic characteristics of dual wing systems*," University of Missouri-Rolla, 1980.

[31] D. W. Fanjoy, and D. J. Dorney, "*Numerical simulations of tandem-airfoil aerodynamics*," presented at the Aerospace Atlantic Conference & Exposition, p. 961295, May 1996.

[32] T. M. Faure, L. Hétru, and O. Montagnier, "Aerodynamic features of a two-airfoil arrangement," *Experiments in Fluids*, vol. 58, no. 10, pp. 146, Oct 2017.

[33] B. Yin, Y. Guan, A. Wen, N. Karimi, and M. H. Doranehgard, "Numerical simulations of ultra-low-Re flow around two tandem airfoils in ground effect: isothermal and heated conditions," *Journal of Thermal Analysis and Calorimetry,* vol. 145, no. 4, pp. 2063-2079, Aug 2021.

[34] M. Delikan, "Computational analysis of 2D foils with and without ground effect in tandem," Master Thesis, *Istanbul Technical University*, İstanbul, 2024.

[35] M. Delikan, and S. Bal, "*Moderate-reynolds number flow around tandem foils with ground effect by CFD,*" presented at the 3rd International Shipbuilding and Maritime Technology Congress (GMO - Shipmar 2024), Trabzon, 2024.

[36] F. R. Menter, "Two-equation eddy-viscosity turbulence models for engineering applications," *AIAA Journal*, vol. 32, no. 8, pp. 1598-1605, Aug 1994.

[37] H. Tennekes, and J. L. Lumley, *A first course in turbulence*, Nachdruck des Originals von 1972. Cambridge, Massachusetts: The MIT Press, 1972.

[38] A. Aslani, A. Shires, A. Shahsavari, and K. C. Kim, "Short-takeoff marine vehicle with circulation flow control of wing-in-ground effect," *Ocean Engineering*, vol. 262, pp. 112074, Oct 2022.

[39] H. Zhi, T. Xiao, S. Deng, M. Tong, P. Chen, and B. Wu, "Distinct wing-in-ground effect of airfoil in proximity to water waves", *AIAA Journal,* vol. 60, no. 6, pp. 3789-3804, Jun 2022.

[40] Y.-H. Im and K.-S. Chang, "Unsteady aerodynamics of a wing-in-ground-effect airfoil flying over a wavy wall", *Journal of Aircraft*, vol. 37, no. 4, pp. 690-696, Jul 2000.

[41] J. Winslow, H. Otsuka, B. Govindarajan, and I. Chopra, "Basic understanding of airfoil characteristics at low reynolds numbers (104-105)", *Journal of Aircraft*, vol. 55, no. 3, pp. 1050-1061, May 2018.

[42] A. O. Nuhait, and D. T. Mook, "Numerical simulation of wings in steady and unsteady ground effects," *Journal of Aircraft,* vol. 26, no. 12, pp. 1081-1089, Dec 1989.

[43] D. Biermann, and W. H. Herrnstein Jr., "The interference between struts in various combinations," *NACA*, United States, Technical Report NACA-TR-468, Jan 1934.